ORNL/TM--11326

DE90 004392

ORNL/TM-11326

Instrument and Controls Division

BILATERAL FORCE REFLECTION FOR TELEOPERATORS WITH MASTERS AND SLAVES WITH DISSIMILAR AND POSSIBLY REDUNDANT KINEMATICS

J. F. Jansen
S. M. Babcock

Date Prepared: October 1989
Date Published: November 1989

NOTICE This document contains information of a preliminary nature. It is subject to revision or correction and therefore does not represent a final report.

Work performed for
Armstrong Aerospace Medical Research Laboratory
Wright-Patterson Air Force Base

Prepared by the
OAK RIDGE NATIONAL LABORATORY
Oak Ridge, Tennessee 37831
operated by
MARTIN MARIETTA ENERGY SYSTEMS, INC.
for the
U.S. DEPARTMENT OF ENERGY
under Contract No. DE-AC05-84OR21400

CONTENTS

ACKNOWLEDGEMENTS

The authors wish to thank Capt. Ronald G. Julian, Capt. Mark S. Jaster, and 1LT Steven J. Remis of the Biological Acoustics Branch, Biodynamics and Bioengineering Division, Armstrong Aerospace Medical Research Laboratory, Wright-Patterson Air Force Base, for their direction and financial support of this work.

ABSTRACT

Several bilateral control techniques and methods for exploiting redundant slaves are investigated as a part of research to develop and analyze bilateral, force-reflecting control methodologies for teleoperator systems with kinematic dissimilar masters and slaves. The study indicates that, with force/torque sensing at the wrist, and an impedance type of controller with the appropriate joint compensation, a significant improvement in performance and controllability of a teleoperator system can be achieved.

1. INTRODUCTION

Bilateral, force-reflecting teleoperators have traditionally consisted of a 6-degree-of-freedom (6-DOF) slave manipulator and a master manipulator with identical kinematic structure. Two basic control structures have been used for force-reflecting manipulators. The first, a position-position control loop, utilizes the position error between the corresponding joints of the master and slave to drive the slave toward the desired position and to provide a retarding force at the master. The second, a position-force control loop, utilizes both the position and torque measurements at each of the joints (or motor drives, in the case of coupled drive systems). The joint (or motor) position error between master and slave is utilized to drive the slave toward the desired position, while the joint (or motor) torque error between the master and slave is utilized to drive the master backward to produce the reflected force.

At least 6-DOF are required to position and orient a manipulator end-effector in space. The addition of a redundant degree of freedom allows for (potentially) an infinite number of manipulator configurations. Criteria to select the best manipulator configuration can be based on a number of performance criteria such as minimizing actuator torques, maximizing end-effector forces, and maximizing end-effector velocities. Significant improvement in the performance of the manipulator can be achieved by means of a redundant manipulator. Dissimilar master-slave systems with nonkinematic replica masters have been used only in research laboratories.

The primary objectives of this research are to develop and analyze bilateral, force-reflecting, control methodologies for teleoperator systems with kinematic dissimilar masters and slaves and to study the performance advantages of redundant slaves. Several bilateral control techniques are investigated in this report along with methods to exploit the redundancy of the slave.

2. REDUNDANT MANIPULATOR DYNAMICS

The dynamic equations of motion for all rigid-bodied link manipulators can be formulated[1] assuming that the gravity component has already been compensated (i.e., by feedforward compensation), as

$$M(q)\ddot{q} + C(q,\dot{q})\dot{q} + J(q)^T F_{ext} = \tau \quad , \tag{2.1}$$

where

$M(q) \in \mathbf{R}^{n\times n}$ is the inertia matrix,

$C(q,\dot{q}) \in \mathbf{R}^{n\times n}$ includes the Coriolis and centrifugal effects,

$J(q) \in \mathbf{R}^{6\times n}$ is the manipulator Jacobian,

$F_{ext} \in \mathbf{R}^6$ is the contact force/torque vector,

$\tau \in \mathbf{R}^n$ is the joint torque vector,

$q \in$ is the generalized joint coordinates,

n = number of degrees of freedom of the manipulator.

For the rest of this report, the functional dependency of M, C, and J will be dropped to reduce the notational clutter.

The task required to be performed by the manipulator, however, is more conveniently represented in Cartesian coordinates. The dynamic equations of motion for the manipulator can be reformulated[1,2] into Cartesian space, $x \in \mathbf{R}^6$, for redundant manipulators as

$$M_x\ddot{x} + C_x\dot{q} + F_{ext} = F \quad , \tag{2.2}$$

where

$M_x = (JM^{-1}J^T)^{-1}$,

$C_x = M_x(JM^{-1}C - \dot{J})$,

$F = M_xJM^{-1}\tau$.

The proof as follows.

Starting with the original joint equation,

$$M\ddot{q} + C\dot{q} + J^TF_{ext} = \tau \quad . \tag{2.3}$$

Multiply by M inverse, since it always exists, to obtain

$$\ddot{q} + M^{-1}C\dot{q} + M^{-1}J^{T}F_{ext} = M^{-1}\tau \quad . \tag{2.4}$$

Now multiply Eq. (2.4) by J :

$$J\ddot{q} + JM^{-1}C\dot{q} + JM^{-1}J^{T}F_{ext} = JM^{-1}\tau \quad . \tag{2.5}$$

Substitution of $J\ddot{q} = \ddot{x} - \dot{J}\dot{q}$ into the above equation results in

$$\ddot{x} - \dot{J}\dot{q} + JM^{-1}C\dot{q} + JM^{-1}J^{T}F_{ext} = JM^{-1}\tau \quad . \tag{2.6}$$

Defining $M_x^{-1} = JM^{-1}J^{T}$, then Eq. (2.6) becomes

$$\ddot{x} - \dot{J}\dot{q} + JM^{-1}C\dot{q} + M_x^{-1}F_{ext} = M_x^{-1}F \quad , \tag{2.7}$$

where

$$F = M_x JM^{-1}\tau.$$

The workspace will include only the region where M_x exists. It should be noted that this restriction is a very mild one and will exclude only singularity points of the manipulator Jacobian. Multiplying Eq. (2.7) by M_x gives

$$M_x\ddot{x} - M_x\dot{J}\dot{q} + M_xJM^{-1}C\dot{q} + F_{ext} = F \quad , \tag{2.8}$$

which can be simplified by combining terms involving $\dot{q}$ and using the definition for C_x in Eq. (2.2). If these simplifications are performed, Eq. (2.8) reduces to

$$M_x\ddot{x} + C_x\dot{q} + F_{ext} = F \quad . \tag{2.9}$$

This concludes the proof.

Since the manipulator is redundant, an infinite number of actuator torque solutions can achieve a dynamic force F at the end-effector, such as,

$$\tau = J^{T}F + (C_s - J_s^{T}M_x\dot{J}_s)\dot{q}_s + M(I - J^{+}J)\Gamma_0 \quad , \tag{2.10}$$

where

J^{+} = the generalized inverse for the manipulator Jacobian[3],

Γ_0 = is an arbitrary joint torque vector.

The first term in Eq. (2.10) will generate the dynamic force required. The second term will compensate for the $C_x\dot{q}_s$ term in Eq. (2.9), and the last term will allow the redundancy of the manipulator to be exploited without causing motion of the end-effector[1,2].

The proof is relatively simple: substitute Eq. (2.10) into Eq. (2.6) and use the definitions for M_x and J^+. Eq. (2.9) then results.

It is interesting to note that if one uses a generalized inverse that minimizes the kinetic energy of the system,[3] Eq. (2.10) simplifies to

$$\tau = J^T F + (C_s - J_s^T M_x \dot{J}_s)\,\dot{q}_s + (I - J^T \bar{J}^T)\,\Gamma_0' \quad , \tag{2.11}$$

where

$\bar{J}$ = the generalized inverse that minimizes kinetic energy,

Γ_0' = an arbitrary joint torque vector.

Proof: Eq. (2.10) can be rewritten as

$$\tau = J^T F + (C_s - J_s^T M_x \dot{J}_s)\,\dot{q}_s + (I - MJ^+JM^{-1})M\Gamma_0 \quad . \tag{2.12}$$

From ref. 3, the generalized inverse that minimizes the kinetic energy is

$$\bar{J} = M^{-1}J^T[JM^{-1}J^T]^{-1} \quad . \tag{2.13}$$

Inserting $\bar{J}$ into Eq. (2.12) for J^+ gives

$$\tau = J^T F + (C_s - J_s^T M_x \dot{J}_s)\,\dot{q}_s + (I - J^T \bar{J}^T)\,M\,\Gamma_0 \quad . \tag{2.14}$$

Since both Γ_0 and Γ_0' are arbitrary and M is nonsingular, replace $M\Gamma_0$ with Γ_0':

$$\tau = J^T F + (C_s - J_s^T M_x \dot{J}_s)\,\dot{q}_s + (I - J^T \bar{J}^T)\,\Gamma_0' \quad , \tag{2.15}$$

This result is identical to Khatib's results in ref. 1.

For avoiding obstacles and joint limits, manipulator redundancy can be used. Since redundancy comes into the force or moment equations as shown in Eq. (2.10), the artificial potential field approach[2] is taken. Obstacles and joint limits that can be best described in joint angles will be represented as potential functions in terms of the joint angles for the manipulator. Let the arbitrary joint torque vector Γ_0 be set as:

$$\Gamma_0 = -\text{grad}[U_q] \quad , \tag{2.16}$$

where

U_q = joint potential function.

As an example, to avoid joint limits, set the potential function[4] to

$$U_q = \begin{cases} 0.5\eta \dfrac{1}{(q_i - q_i^d)^2}, & \text{if } |q_i - q_i^d| \le \text{tresh}_i \\ \\ 0, & \text{otherwise} \end{cases} , \tag{2.17}$$

where

η = a positive constant that determines the strength of the potential force,

q_i^d = the i^{th} joint limit,

tresh_i = the i^{th} joint threshold.

The total joint potential of all the joints is simply a superposition of each of the individual joint potential functions.

If the elbow of the arm has to avoid a certain region in the workspace, the joint potential function can be written in a similar manner. Also, for the situation in which the elbow of the manipulator is required to track the elbow of the operator as closely as possible, a simple (spring-like) potential function can be created, such as

$$U_q = 0.5(x_{elbow} - x^D_{elbow})^T K_s (x_{elbow} - x^D_{elbow}) , \tag{2.18}$$

where

x_{elbow} = elbow Cartesian position of the slave,

x^D_{elbow} = elbow Cartesian position of the master,

K_s = weighting matrix of desired spring constants.

Arbitrary joint torque vector Γ_0 is defined as in Eq. (2.16), which, after some algebraic manipulation, simplifies to

$$\Gamma_0 = -J^T_{elbow} K_s (x_{elbow} - x^D_{elbow}) , \tag{2.19}$$

where J_{elbow} is the Jacobian of the slave elbow.

Further, it might be desirable either to improve the manipulator mechanical advantage (MMA) or the manipulator velocity ratio (MVR)[5,6] through the redundancy of the manipulator. For the MMA case, the joint torque vector should be set as

$$\Gamma_0 = -k(J_m^T u_m)^T \frac{\partial \left(J_m{}^T u_m \right)}{\partial q_i} , \tag{2.20}$$

where

k = positive constant that determines the strength of the potential force,

u_m = known unit vector in the direction of the force to be applied by the end-effector,

$J_m = W_f^{-1/2} J W_\tau^{1/2}$ where $W_f^{-1/2}$ and $W_\tau^{1/2}$ are positive definite and symmetric weighting matrices,

J = manipulator Jacobian.

Likewise, for the MVR case, the joint torque vector should be set as

$$\Gamma_0 = k\left(J_v^T z\right)^T \frac{\partial\left(J_v^T z\right)}{\partial q_i} \quad , \tag{2.21}$$

where

k = the positive constant that determines the strength of the potential force,

$z = (J_v J_v^T)^{-1} u_v$,

u_v = known unit vector in the direction of the desired velocity of the end-effector,

$J_v = W_x^{1/2} J W_\theta^{-1/2}$ where $W_x^{1/2}$ and $W_\theta^{-1/2}$ are positive definite and symmetric weighting matrices,

Finally, asymptotic stability of a redundant manipulator requires that a dissipation force be selected that acts in the null space of the Jacobian matrix.[1] This dissipation force will be inserted into the Γ_0 term in Eq. (2.11) in the following form:

$$\Gamma_0 = -k_{vnull} M \dot{q} \quad . \tag{2.22}$$

A summary is listed in Table 1 of possible joint torque vectors, Γ_0, that exploit the redundancy of a manipulator. It should be mentioned that the entry in Table 1 pertaining to the null motion stabilization[1] is required for all redundant manipulators, not an option. Care should be taken to ensure that the arbitrary joint torque vector does not excite any of the resonant modes of the manipulator. Suitable filtering could be added to compensate for this potential problem. Finally, combinations of desirable attributes (such as joint avoidance and elbow tracking) can be simply combined to form a new joint torque vector signal. An unsolved research problem that has to be addressed is the determination of the relative weights among different schemes.

Table 1. Possible ways of utilizing the manipulator redundancy

1. Obstacle and joint avoidance:

$$U_q = \begin{cases} 0.5\eta \dfrac{1}{q_i - q_i^{d\,2}}, \text{ if } |q_i - q_i^d| \le \text{tresh}_i \\ \\ 0, \text{ otherwise} \end{cases},$$

and

$$\Gamma_0 = -\text{grad}[U_q] \quad .$$

2. Elbow tracking:

$$\Gamma_0 = -J_{elbow}^T K_s (x_{elbow} - x_{elbow}^D) \quad .$$

3. Mechanical advantage:

$$\Gamma_0 = -k(J_m^T u_m)^T \frac{\partial J_m{}^T u_m}{\partial q_i} \quad .$$

4. Velocity ratio:

$$\Gamma_0 = k\left(J_v^T z\right)^T \frac{\partial\left(J_v^T z\right)}{\partial q_i} \quad .$$

5. Null motion stabilization:

$$\Gamma_0 = -k_{vnull} M\dot{q} \quad .$$

3. DESIGN PHILOSOPHY

3.1 INTRODUCTION

For teleoperation, the design problem is difficult because the human operator is in the control loop. The operator will change the dynamics of the master arm in an unknown and unpredictable manner. Therefore, any control scheme for the master, and indirectly for the slave, will be significantly modified by the operator's imposed dynamics. Two possible ways to handle the dynamics of the operator are the probe method and adaptive impedance control.

3.2 PROBE METHOD

The basic idea of the probe method is to control the slave as if it were a mechanical probe with an operator-specified impedance. The master is controlled such that the operator's dynamics dominates and the slave hand forces are fed back through the master Jacobian to give the operator an accurate indication of the slave force. The specific design requirements follow.

1. The slave forces are fed back by means of the master Jacobian,

$$\tau_m = J_m^T (\sigma F_s) + {}^c\tau_m \tag{3.1}$$

where

F_s = measured slave force,

σ = positive force sensitivity constant,

J_m = manipulator Jacobian for the master,

τ_m^c = master controller signal.

2. The master controller excluding the slave force feedback should be gravity-compensated to avoid fatiguing the operator:

$$\tau_m = J_m^T(\sigma F_s) + \tau_{grav} + \tau_m^c \ , \tag{3.2}$$

where

τ_{grav} = torque signal to compensate for gravity effects.

3. Master controller τ_m^c should be stable in the sense that, if the operator released the manipulator and the slave manipulator was locked into a fixed position with F_s set to zero, the master arm should settle to, or close to, the zero positional error posture. The positional error is defined as

$$e = x_m - x_s \quad . \tag{3.3}$$

4. The operator's dynamics should dominate the master arm dynamics, τ_m^c. This statement is somewhat equivalent to Arzbaecher's requirement[7] for a single-joint force-reflecting servo: "For ease in manipulation it is essential that a force-reflecting manipulator require little torque to move the input handle from one place to another when the output handle has no load." This condition also imposes a mechanical design requirement: the master dynamic forces should be relatively small compared to the operator's dynamic forces. This restriction will probably not be possible throughout the master workspace, depending on how close the operator is to his or her singularity point. The operator's singularity points can be avoided by exploiting the redundancy of his or her skeletal frame. The master controller can be a stiffness controller such as

$$\tau_m^c = J^T[K_{pm}(x_s - x_m) + K_{vm}(\dot{x}_s - \dot{x}_m)] \quad , \tag{3.4}$$

where

J = master Jacobian,

K_{pm} and K_{vm} = positional and velocity gain matrices, respectively,

x_s and $\dot{x}_s$ = slave position and velocity, respectively,

x_m and $\dot{x}_m$ = master position and velocity, respectively.

More will be said about the stiffness controller in Sect. 4.

The gain selection should be such that the operator's dynamics dominate and condition 3 is satisfied. Typically, the gain matrices will be diagonal matrices,

$$K_{pm} = \text{diag}(k_{pm}^1,...,k_{pm}^6) \tag{3.5}$$

and

$$K_{vm} = \text{diag}(k_{vm}^1,...,k_{vm}^6) \quad , \tag{3.6}$$

where it is assumed that the master is a 6-DOF manipulator. To ensure stability,

$$k_{pm}^i > 0, \text{ for } i = 1,...,6 \tag{3.7}$$

and

$$k_{vm}^i > 0, \text{ for } i = 1,...,6 \tag{3.8}$$

Further, each gain constant should be set to a small positive value to ensure that the operator's dynamics dominates. The master positional gain matrix, which is related by a positive constant to the slave positional gain matrix, will be discussed shortly.

5. The slave controller should be designed as an impedance controller with an actuator signal of

$$\tau_s = J_s^T\{M_x[K_{ps}(x_m - x_s) + K_{vs}(\dot{x}_m - \dot{x}_s)]\} \quad . \tag{3.9}$$

More will be said about the impedance controller in Sect. 4.

6. When coupled together, the master and slave should be stable so that when the master is free from its human operator, the relative positional error, $e = x_m - x_s$, goes to zero as time increases.

When the master is freed by the human operator, the teleoperation system should be dynamically stable so that runaway is avoided. The slave controller will be based on the concept of impedance control because of the desirable properties of decoupled dynamic response, uniform stiffness, and adjustable stiffness (see Sect. 4 for more details). The master controller does not have to be as complicated as the slave controller because the human operator should be the dominant control force, as previously discussed. Using a stiffness controller for the master will provide uniform stiffness throughout the workspace. Further, its use has the desirable property of global stability. The proof (similar to that of ref. 8) follows.

The slave's dynamic equations of motion in Cartesian space are

$$\ddot{x}_s + K_{vs}\dot{x}_s + K_{ps}(x_s - x_m) = 0 \quad , \tag{3.10}$$

where contact forces have been removed. The master's dynamics of motion in Cartesian space [see Eq. (3.6)] is

$$M_{xm}\ddot{x}_m + K_{vm}\dot{x}_m + K_{pm}(x_m - x_s) + C_{xm}\dot{q}_m = 0 \quad , \tag{3.11}$$

where M_{xm} and C_{xm} are the Cartesian inertia and centrifugal/Coriolis terms, respectively.

Define a Liapunov candidate function[9] L as

$$L = 0.5\alpha\dot{x}_s^T\dot{x}_s + 0.5\dot{x}_m^TM_{xm}\dot{x}_m + 0.5(x_m - x_s)^TK_{pm}(x_m - x_s) \quad , \tag{3.12}$$

where $\alpha > 0$ is an arbitrary positive constant. Taking the derivative of L with respect to time:

$$\dot{L} = \alpha\dot{x}_s^T\ddot{x}_s + \dot{x}_m^TM_{xm}\ddot{x}_m + 0.5\dot{x}_m^T\dot{M}_{xm}\dot{x}_m + (x_m - x_s)^TK_{pm}(\dot{x}_m - \dot{x}_s) \quad . \tag{3.13}$$

Substituting Eqs. (3.10) and (3.11) into Eq. (3.13) results in the following:

$$\dot{L} = -\alpha\dot{x}_s^TK_{vs}\dot{x}_s - \dot{x}_m^TK_{vm}\dot{x}_m + 0.5\dot{x}_m^T\dot{M}_{xm}\dot{x}_m - \dot{x}_m^TC_{xm}\dot{q}_m \quad , \tag{3.14}$$

where

$$K_{pm} = \alpha K_{ps} \tag{3.15}$$

has been used to provide the stability constraint between the master and slave controller.

Since our objective is to show that $\dot{L}$ is negative semidefinite, which would be true if the last two terms in Eq. (3.14) were zero, make the following definition:

$$\xi \equiv 0.5\dot{x}_m^T \dot{M}_{xm} \dot{x}_m - \dot{x}_m^T C_{xm} \dot{q}_m \quad . \tag{3.16}$$

This expression for ξ will now be shown to be zero.

Using the definition of the manipulator Jacobian, Eq. (3.16) can be rearranged into

$$\xi = 0.5\dot{q}_m^T [J_m^T \dot{M}_{xm} J_m - J_m^T C_{xm}] \dot{q}_m \tag{3.17}$$

or

$$\xi = 0.5\dot{q}_m^T \Lambda \dot{q}_m \quad , \tag{3.18}$$

where

$$\Lambda = [J_m^T \dot{M}_{xm} J_m - J_m^T C_{xm}] \quad .$$

Using the fact that $\dot{M}_m - 2C_m$ is a skew symmetric matrix, and after some messy algebraic manipulation, it can be shown that Λ is also skew symmetric. If Λ is skew symmetric, then ξ is 0[10].

Eq. (3.14) reduces to

$$\dot{L} = -\alpha \dot{x}_s^T K_{vs} \dot{x}_s - \dot{x}_m^T K_{vm} \dot{x}_m \leq 0 \quad , \tag{3.19}$$

which shows that $\dot{L}$ is negative semidefinite. Two cases need to be examined when $\dot{L} = 0$ (i.e., $\dot{x}_s = 0$ and $\dot{x}_m = 0$) to show that $e = x_m - x_s \dashrightarrow 0$ as time increases.

Case 1: If $e = x_m - x_s = 0$, then convergence has been shown.

Case 2: If $e = x_m - x_s \neq 0$, then from Eqs. (3.10) and (3.11),

$$\ddot{x}_s = K_{ps} e \neq 0 \tag{3.20}$$

and

$$\ddot{x}_m = -M_{xm}^{-1} K_{pm} e \neq 0 \quad , \tag{3.21}$$

where singularity points are assumed to be avoided. Since the slave and master accelerations are not zero, their respective velocities will not stay at zero; that is,

$$\dot{x}_s \cong \Delta t \ddot{x}_s \text{ and } \dot{x}_m \cong \Delta t \ddot{x}_m \quad , \tag{3.22}$$

where Δt = time. Therefore, $\dot{L} < 0$, which means that e---> 0 as time increases, which concludes the proof.

It is interesting to note that if the slave controller was a stiffness controller, global stability could still be shown[8]. This proof shows that the slave and master controller can be analyzed separately, since together they are stable.

3.3 ADAPTIVE IMPEDANCE CONTROL

The other method to control a teleoperated system can be described as follows.

The operator arm is assumed to behave like a variable impedance manipulator. The operator can change at will the setting of his arm stiffness and relative damping. The master controller will try to estimate the operator impedance in real time. With this estimation, the slave impedance will be changed to the estimated value of the operator. Further, the slave force will be sent to the master. Both the master and slave will require a force torque transducer, as opposed to the probe method that needs a force torque transducer only at the slave.

The technical difficulty with the adaptive impedance control method is that it assumes a physiological model (i.e., an impedance model) for the operator which to this date is still unknown. Further, a force/torque sensor on the master end-effector is required. Because of these restrictions, only the probe method is deemed technically feasible at this phase of the research and will be the only method elaborated upon.

4. OVERVIEW OF PAST WORK

4.1 INTRODUCTION

Four major classes of force control schemes have been proposed for robotic applications. Each can be modified to handle the master/slave teleoperation problem. For simplicity, only the slave control algorithm will be given, since the master controller, as discussed in the previous section, can be described as

$$\tau_m = J_m^T(\sigma F_s) + \tau_m^c \tag{4.1}$$

and can be treated separately.

For each of the four classes it will be assumed that the slave is a redundant manipulator, which means that a change to the nonredundant manipulator case can be made simply by replacing J_s^+ or $\bar{J}_s$ to J_s^{-1} and making the necessary simplifications. Using results from Sect. 2, each controller will be discussed based on the transient, stability, and stiffness attributes of the slave in Cartesian space.

4.2 POSITION-POSITION CONTROL

For position-position control, the torque signal can be produced in a number of different ways. Normally, the null space torque signal τ_{null} is not explicitly included in the torque signal and can be written as follows[4,5]:

$$\tau_s = K_{ps}(q_s^D - q_s) + K_{vs}(\dot{q}_s^D - \dot{q}_s) + \tau_{sgrav} \ , \tag{4.2}$$

where

$$\dot{q}_s^D = J_s^+ \dot{x}_m + (I - J_s^+ J_s)\Gamma_0 \ , \tag{4.3a}$$

$$q_s^D = \int_0^t \dot{q}_s^D d\xi \ . \tag{4.3b}$$

Insert Eq. (4.2) into Eq. (2.6). After some simplifications, the equation of motion in Cartesian space will be

$$M_X \ddot{x}_s + \bar{J}_s^T K_{vs} (\dot{q}_s - \dot{q}_s^D) + \bar{J}_s^T K_{ps}(q_s - q_s^D) + F_{sext} + C_x \dot{q}_s = 0 \ . \tag{4.4}$$

Notice that an expression similar to the null space torque signal appears in Eq. (4.4) by means of Eqs. (4.3a) and (4.3b). This appearance potentially could cause instability, both in the Liapunov and in the practical sense, because:

1. The signal $(I - J_s^+ J_s)\Gamma_0$ could have a significant frequency component that overlaps one of the resonant frequencies of the manipulator.

2. $(I - J_s^+ J_s)\Gamma_0$ might not be properly bounded, so that potential torque saturation could occur.

3. Damping in the null space will be configuration-dependent and could cause the transient reponse of a particular trajectory to be significantly underdamped.

Further, at steady state, Eq. (4.4) simplifies to

$$\bar{J}_s^T K_{ps}(q_s - q_s^D) + F_{sext} = 0 \quad , \tag{4.5}$$

which indicates that the stiffness seen by the end-effector is dependent on the location of the slave in its workspace. Also, it is clear from Eq. (4.4) that coupling will occur between the different slave states, indicating that the transient response of the end-effector will be complex. An eigenvalue analysis of the linearization of Eq. (4.4) indicated that the eigenvalues will move significantly in the left half of the s plane[11]. A simple quantitative measure of the variation of the eigenvalues is the average or mean eigenvalue defined as

$$\sigma \equiv \frac{\sum_{i=1}^{2n} \lambda_i}{2n} = \frac{-\text{Trace}(M_s^{-1} K_{vs})}{2n} \quad . \tag{4.6}$$

The mean eigenvalue can easily vary by 100% in the workspace.[11]

Global stability can be proven for this controller under certain conditions and will be given in Sect. 5.

4.3 HYBRID CONTROL

The hybrid controller[12] torque signal can be described as

$$\tau_s = K_{ps} J_s^+(x_m - x_s) + K_{vs} J_s^+(\dot{x}_m - \dot{x}_s) + \tau_{null} + \tau_{sgrav} \quad , \tag{4.7}$$

where

τ_{null} = null space torque signal of the following form $(I - J_s^+ J_s)\Gamma_0$,

τ_{sgrav} = slave gravitational torque compensation signal,

J_s^+ = least-square generalized inverse.

Insert Eq. (4.7) into Eq. (2.6). After some simplifications, the equation of motion in Cartesian space will be

$$M_X \ddot{x}_s + \bar{J}_s^T K_{vs} J_s^+(\dot{x}_s - \dot{x}_m) + \bar{J}_s^T K_{ps} J_s^+(x_s - x_m) + \bar{J}_s^T \tau_{null} + F_{sext} + C_x \dot{q}_s = 0 \quad . \tag{4.8}$$

The null space torque signal does not disappear in Eq. (4.8). Further, at steady state, Eq. (4.8) simplifies to

$$\overline{J}_s^T K_{ps} J_s^+ (x_s - x_m) + F_{sext} = 0 \quad , \tag{4.9}$$

which indicates that the stiffness as seen by the end-effector will change, depending on the location of the slave in its workspace. Also, it is clear from Eq. (4.8) that coupling will occur between the different slave states, indicating that the transient response of the end-effector will be very complex. The variation of the eigenvalues for the linearization of Eq. (4.8) in joint space will be identical to that of position-position control for the nonredundant manipulator case and will not be repeated[11].

While, to the author's knowledge, global stability has not been proven for this controller, local stability can be proven for small perturbations from the equilibrium points. This local stability proof will be given in Sect. 5.

4.4 STIFFNESS CONTROL

For stiffness control,[13] the torque signal is

$$\tau_s = J_s^T [K_{ps}(x_m - x_s) + K_{vs}(\dot{x}_m - \dot{x}_s)] + \tau_{null} + \tau_{sgrav} \quad , \tag{4.10}$$

with the null space torque signal defined as for the last case (i.e., $\tau_{null} = (I - J_s^+ J_s)\Gamma_0$). Insert Eq. (4.10) into Eq. (2.6). After some simplifications, the equation of motion in Cartesian space will be

$$M_x \ddot{x}_s + K_{vs}(\dot{x}_s - \dot{x}_m) + K_{ps}(x_s - x_m) + \overline{J}_s^T \tau_{null} + F_{sext} + C_x \dot{q}_s = 0 \quad . \tag{4.11}$$

Notice that the null space torque signal again appears in Eq. (4.11). At steady state, Eq. (4.11) simplifies to

$$K_{ps}(x_s - x_m) + F_{sext} = 0 \quad , \tag{4.12}$$

which indicates that the stiffness seen by the end-effector is independent of the location of the slave in its workspace. Also, it is clear from Eq. (4.11) that there will still be coupling between the different slave states (because M_x typically will not be a diagonal matrix), indicating that the transient response of the end-effector will again be very complex. An eigenvalue analysis of the linearization of Eq. (4.11) in joint space indicates that the eigenvalues will move again significantly in the left half of the s plane.[11] The mean eigenvalue[14] is defined as

$$\sigma \equiv \frac{\sum_{i=1}^{2n} \lambda_i}{2n} = \frac{-\text{Trace}(M_s^{-1} J_s^T K_{vs} J_s)}{2n} \quad . \tag{4.13}$$

The mean eigenvalue for stiffness control can vary significantly, but it usually has a value of less than either the position-position or hybrid control[11].

Global stability can be proven for this controller and will be given in Sect. 5.

4.5 IMPEDANCE CONTROL (OR RESOLVED ACCELERATION CONTROL OR OPERATIONAL SPACE METHOD)

For impedance control[1,11,15-18], the torque signal is

$$\tau_s = J_s^T\{M_x[K_{ps}(x_m - x_s) + K_{vs}(\dot{x}_m - \dot{x}_s)]\}$$

$$+ (C_s - J_s^T M_x \dot{J}_s)\dot{q}_s + \tau_{null} + \tau_{sgrav} \quad . \tag{4.14}$$

Insert Eq. (4.14) into Eq. (2.6). After some simplifications, the equation of motion in Cartesian space will be

$$\ddot{x}_s + K_{vs}(\dot{x}_s - \dot{x}_m) + K_{ps}(x_s - x_m) + F_{sext} = 0 \quad . \tag{4.15}$$

Notice that the null space torque signal does not appear in Eq. (4.15), which would not occur if it had a form different from that of $(I - J_s^T \bar{J}_s^T)\Gamma_0$. Further, at steady state, Eq. (4.15) simplifies to

$$K_{ps}(x_s - x_m) + F_{sext} = 0 \quad , \tag{4.16}$$

which indicates that the stiffness seen by the end-effector is independent of the location of the slave in its workspace. Also, it is clear from Eq. (4.15) that no coupling will occur between the different slave states, indicating that the transient response of the end-effector will behave like a decoupled second-order linear differential equation with constant coefficients. Since Eq. (4.15) is already linear, its eigenvalues will not move in the left half of the s plane.[11] Global stability can be proven for this controller and will be given in Sect. 5.

4.6 REDUCED ORDER IMPEDANCE CONTROLLER

The problems with implementing the impedance controller discussed in Sect. 3.5 are related to the computational intensiveness of the algorithm and how to cope with unknown payloads. The reduced-order impedance controller is an attempt to reduce the computational effort while maintaining the desirable properties of an impedance controller. This scheme is not a new type of controller but an approximation of the impedance controller. To reduce the computational intensity of the impedance control algorithm, the velocity terms in Eq. (4.14) associated with Coriolis, centrifugal, and the change in the manipulator Jacobian effects will be ignored, that is,

$$\tau_s = J_s^T\{M_x\,[K_{ps}(x_m - x_s) + K_{vs}(\dot{x}_m - \dot{x}_s)]\} + \tau_{null} + \tau_{sgrav} \quad . \tag{4.17}$$

Equation (4.17) can be rearranged into the following form:

$$z = \bar{J}_s\{[K_{ps}(x_m - x_s) + K_{vs}(\dot{x}_m - \dot{x}_s) - J_sM_s^{-1}\Gamma_0]\} \quad , \tag{4.18}$$

where

$z \equiv M_s^{-1}(\tau_s - \tau_{sgrav} - \Gamma_0)$,

M_s = slave inertia tensor.

If it is assumed that slave inertia tensor is known (more will be said about this later), then everything within the brackets in Eq. (4.18) is known. Equation (4.18) can be solved based on a modification of the scheme proposed by Dubey et al.[4] This modified scheme solves the problem of solving for $\dot{q}_{min}$ given $\dot{x}$, where both are related by the generalized inverse which minimizes the kinetic energy, that is

$$\dot{q}_{min} = \bar{J}_s\dot{x} \quad . \tag{4.19}$$

The modified scheme utilizes the particular solution, $\dot{q}_p$, of Eq. (4.19) and its homogeneous solution, $\dot{q}_h$. Every joint solution to the equation $\dot{x} = J_s\dot{q}$ can be written as a linear combination of the particular and homogeneous solution,

$$\dot{q} = \dot{q}_p + k\dot{q}_h \quad , \tag{4.20}$$

where k is some arbitrary constant. To solve for $\dot{q}_{min}$, k should be set at

$$K = -\frac{\dot{q}_p^{\,T}M_s\dot{q}_h^{\,T}}{\dot{q}_h^{\,T}M_s\dot{q}_h^{\,T}} \quad . \tag{4.21}$$

So, if the inertia tensor is known, then $\dot{q}_{min}$ can be found. If $\dot{x}$ in Eq. (4.19) is replaced with $K_{ps}(x_m - x_s) + K_{vs}(\dot{x}_m - \dot{x}_s) - J_sM_s^{-1}\Gamma_0$, then z can be solved for in Eq. (4.18). The actuator torques then can be determined from z.

$$\tau_s = M_s^{-1}z + \tau_{sgrav} + \Gamma_0 \quad . \tag{4.22}$$

Because of the difficulty in obtaining the inertia tensor and because many of the terms of inertia tensor are not significant, we are proposing to use a sparse inertia tensor with all off-diagonal terms set to zero.

4.7 RANKING OF THE CONTROLLERS

A summary of the attributes of the five controllers is shown in Table 2. Of the five controller types, only the impedance controller has all the desirable attributes of uniform stiffness, decoupled transient response, and global stability in Cartesian space. Next is the stiffness controller, which is somewhat similar to the impedance controller but has somewhat fewer computational requirements than the impedance controller.

Table 2. A summary of the attributes of the five controllers

Controller type	Decoupled transient response	Stability	Constant stiffness	Computational complexity
1. Position-Position	No	Global	No	Low
2. Hybrid	No	Local	No	Moderate
3. Stiffness	No	Global	Yes	Moderate
4. Impedance	Yes	Global	Yes	High
5. ROIC	Approximately	Local	Yes	Moderate

Some comments are necessary at this point. The discussion so far has assumed that the master and slave can be modeled as a kinematic chain of rigid-body objects with ideal actuators. Unfortunately, most mechanical manipulators are far from this ideal, and unmodeled dynamics has a significant effect on their overall performance. These aspects will be discussed in depth in Sect. 6. The purpose of the first five sections is to explain the basis of the problem. Section 6 will discuss ways to compensate for unmodeled dynamics at the joint level that will reduce their effects on the ideal model. Section 5 will examine in more depth the stability of the various controllers summarized in Table 2. This section can be skipped without any loss of continuity.

5. STABILITY AND TRANSIENT ANALYSIS

5.1 INTRODUCTION

Each of the controller types will be discussed, as mentioned in the previous section, concerning their stability and transient properties. This section can be skipped by the reader without any loss of continuity.

5.2 STIFFNESS CONTROL

5.2.1 Global Positional Stability

For position control, assume that the master is fixed and the slave is required to track the master, that is

$$\begin{pmatrix} x_s \\ \dot{x}_s \end{pmatrix} \rightarrow \begin{pmatrix} x_m \\ 0 \end{pmatrix} \text{ as } t \rightarrow \infty \ .$$

The slave actuator torque signal for stiffness control can be represented as

$$\tau_s = J_s^T \left[K_{ps}(x_m - x_s) + K_{vs}(\dot{x}_m - \dot{x})\right] + (I - J_s^+ J_s)\, \Gamma_0 \tag{5.1}$$

and

$$\Gamma_0 = - k_{vnull} \dot{q}_s + \Gamma_0' \tag{5.2}$$

where

k_{vnull} = a fixed positive constant,

Γ_0' = an additional torque signal for such elements as obstacle avoidance and torque minimization, as discussed in Sect. 2.

For notational simplicity, let $P = (I - J_s^+ J_s)\, \Gamma_0$, where P has all the properties of a projection matrix. Gravity compensation is assumed to be included in Eq. (5.1), but for simplicity it will not be shown.

To show positional stability of stiffness control, a Liapunov function candidate[9] can be written as

$$V(\Delta x, \dot{q}_s) = 0.5\ \dot{q}_s^T M_s\ \dot{q}_s^T + 0.5\ (\Delta x)^T K_{ps}(\Delta x) \ , \tag{5.3}$$

where

$$\Delta x = x_m - x_s \ ,$$

$$K_{ps} > 0 \ .$$

V is a continuously differentiable positive definite function in terms of Δx and $\dot{q}_s$. According to Liapunov's second method,[9] one needs to show for global stability that

$$\frac{dV}{dt} = \dot{V} < 0 \tag{5.4}$$

for all nontrivial trajectories. This derivative will be proved as follows.

Taking the derivative of Eq. (5.3),

$$\dot{V} = \dot{q}_s^T M_s \ddot{q} + 0.5 \ \dot{q}_s^T \dot{M}_s \dot{q}_s - \dot{x}_s^T K_{ps}(x_m - x_s) \ . \tag{5.5}$$

Substitute $M_s \ddot{q}_s = \tau_s - C_s \dot{q}_s$ into Eq. (5.5):

$$\dot{V} = \dot{q}_s^T(\tau_s - C_s\dot{q}_s) + 0.5 \ \dot{q}_s^T \dot{M}_s \dot{q}_s - \dot{x}_s^T K_{ps}(x_m - x_s) \ . \tag{5.6}$$

Collecting like terms,

$$\dot{V} = \dot{q}_s^T(\tau_s) + 0.5 \ \dot{q}_s^T(\dot{M}_s - 2C_s) \ \dot{q}_s - \dot{x}_s^T \ K_{ps}(x_m - x_s) \ . \tag{5.7}$$

Since $\dot{M}_s - 2C_s$ is an antisymmetric matrix,[10]

$$\dot{q}_s^T(\dot{M}_s - 2 \ C_s) \ \dot{q}_s = 0 \ ; \tag{5.8}$$

then,

$$\dot{V} = \dot{q}_s^T(\tau_s) - \dot{x}_s^T K_{ps}(x_m - x_s) \ . \tag{5.9}$$

Substituting Eq. (5.1) into Eq. (5.9) gives the following:

$$\dot{V} = \dot{q}_s^T\{J_s^T[K_{ps}(x_m - x_s) + K_{vs}(\dot{x}_m - \dot{x}_s)] + P \ \Gamma_0\} - \dot{x}_s^T K_{ps}(x_m - x_s) \ . \tag{5.10}$$

Exploiting the fact that $J_s\dot{q}_s = \dot{x}_s$, inserting this equation into Eq. (5.10) and replacing $\dot{x}_m = 0$ gives

$$\dot{V} = -\dot{x}_s^T K_{vs} \ \dot{x}_s + \dot{q}_s^T \ P \ \Gamma_0 \ . \tag{5.11}$$

Now insert Eq. (5.2) into Eq. (5.11):

$$\dot{V} = -\dot{x}_s^T K_{vs} \ \dot{x}_s + \dot{q}_s^T P(-k_{vnull}\dot{q}_s + \Gamma_0') \ . \tag{5.12}$$

Using the fact that k_{vnull} is a positive constant, Eq. (5.12) can be modified to:

$$\dot{V} = -\dot{x}_s^T K_{vs} \dot{x}_s - k_{vnull} \dot{q}_s^T P \dot{q}_s + \dot{q}_s^T P \Gamma_0' \quad . \tag{5.13}$$

Assuming that $\Gamma_0' = 0$, which means that the redundancy is not being exploited, simplifies Eq. (5.13) to

$$\dot{V} = -\dot{x}_s^T K_{vs} \dot{x}_s - k_{vnull} \dot{q}_s^T P \dot{q}_s \quad . \tag{5.14}$$

Define the projection matrix $Q = J_s^+ J_s$. Both P and Q are projection matrices, have the properties that $L = \{P\ v: v \in R^n\}$ and $L^\perp = \{Q\ v: v \in R^n\}$, and are orthogonal linear subspaces.[19] Further, any point $v \in R^n$ can be represented uniquely as $v = p + q$, where $p \in L$ and $q \in L^\perp$. Decompose $\dot{\delta} q_s$ into

$$\dot{\delta} q_s = \dot{\delta} q_s^\perp + \dot{\delta} q_s^{null} \quad . \tag{5.15}$$

where $\dot{\delta} q_s^\perp \in L^\perp$ and $\dot{\delta} q_s^{null} \in L$. Then Eq. (5.14) simplifies to

$$\dot{V} = -(\dot{\delta} q_s^\perp)^T J_s^T K_{vs} J_s (\dot{\delta} q_s^\perp) - k_{vnull} (\dot{\delta} q_s^{null})^T (\dot{\delta} q_s^{null}) \quad . \tag{5.16}$$

Equation (5.16) indicates that $\dot{V} < 0$ for $\dot{q}_s \neq 0$ and $K_{vs} > 0$.

Up to this point, all that has been shown is that $\dot{V}$ is negative semidefinite and not the negative definite needed to prove global stability. The following argument will show that $\dot{V}$ is negative definite.

For $\dot{q}_s = 0$, $\dot{V} = 0$, which means that there are two possible cases to consider, either $\Delta x = 0$ or $\Delta x \neq 0$. If $\Delta x = 0$, then $V = 0$, which means that we are at the desired point. Further, $\tau_s = 0$, which means that the actuator will not try to move from this point.

If $\Delta x \neq 0$, then $V \neq 0$, since V is positive definite. Further,

$$M_s \ddot{q}_s = \tau_s = J_s^T K_{ps} \Delta x \tag{5.17}$$

or

$$\ddot{q}_s = M_s^{-1} \tau_s = M_s^{-1} J_s^T K_{ps} \Delta x \quad . \tag{5.18}$$

Now there are two possibilities: $\ddot{q}_s \neq 0$ and $\ddot{q}_s = 0$. For $\ddot{q}_s = 0$, this means that $M_s^{-1} J_s^T K_{ps}$ is singular, which can be explained physically as requiring the manipulator to move in a direction in which it cannot move. Thus the case of $\ddot{q}_s = 0$ is not of interest because it is physically unrealizable.

For $\ddot{q}_s \neq 0$,

$$\dot{q}_s \cong \Delta t\ \ddot{q}_s \quad , \tag{5.19}$$

which means that $\dot{V} < 0$ since $\dot{q}_s \neq 0$ from Eq. (5.19). This means that the stall condition of $\dot{q}_s = 0$ and $\Delta x \neq 0$ is not a stable equilibrium point. Therefore, the positional stability of the stiffness controller has been shown.

5.2.2 Force Stability

When the slave is in contact with a surface, it will feel an external force. Assuming that the master position is fixed, let the external force be represented as an elastic restoring force,

$$F_{sE} = K_E(x_s - x_E) \quad , \tag{5.20}$$

where K_E is the environment stiffness constant.

The dynamic equation of motion for the slave can be represented as

$$M_s \ddot{q}_s + C_s \dot{q}_s + J_s^T F_{sE} = \tau_s \quad . \tag{5.21}$$

Inserting Eqs. (5.1), (5.2), and (5.20) into Eq. (5.21) gives

$$M_s \ddot{q}_s + C_s \dot{q}_s + J_s^T K_E(x_s - x_E)$$

$$= J_s^T[K_{ps}(x_m - x_s) + K_{vs}(\dot{x}_m - \dot{x}_s)] - k_{vnull}(I - J^+J)M_s \dot{q}_s \quad . \tag{5.22}$$

After collecting like terms, Eq. (5.22) becomes

$$M_s \ddot{q}_s + C_s \dot{q}_s + J_s^T[(K_{ps} + K_E)(x_m' - x_s) + K_{vs}(\dot{x}_m - \dot{x}_s)] - k_{vnull}(I - J^+J)M_s \dot{q}_s \quad , \tag{5.23}$$

where $x_m' = (K_{ps} + K_E)^{-1}(K_{ps} x_m + K_E x_E)$.

Since K_E is positive definite, the stability proof is identical for the positional case. However, the stable equilibrium point will now be x_m' instead of x_m.

5.3 IMPEDANCE CONTROL

The slave actuator torque signal for impedance control can be represented as

$$\tau_s = J_s^T M_x[K_{ps}(x_m - x_s) + K_{vs}(\dot{x}_m - \dot{x}_s)] + (C_s - J_s^T M_x \dot{J}_s)\dot{q}_s + M_s(I - J^+J)\Gamma_0 \quad . \tag{5.24}$$

Gravity compensation is again assumed to be included in Eq. (5.24) but for simplicity it will not be shown.

To show global positional stability of the end-effector, a Liapunov function candidate can be written as

$$V(\Delta x, \dot{x}_s) = 0.5\, \dot{x}_s^T \dot{x}_s + 0.5\, (\Delta x)^T K_{ps}(\Delta x) \quad , \tag{5.25}$$

where

$$\Delta x = x_m - x_s \ ,$$

$$K_{ps} > 0 \ .$$

Taking the derivative of Eq. (5.25) results in

$$\dot{V} = \dot{x}_s^T \ddot{x} + (\Delta x)^T K_{ps}(\dot{\Delta x}) \ . \tag{5.26}$$

Substituting Eq. (5.24) into Eq. (2.16) and then substituting the resulting expression for $\ddot{x}_s$ into Eq. (5.26) results in

$$\dot{V} = -\dot{x}_s^T K_{vs} \dot{x}_s \ , \tag{5.27}$$

which indicates that $\dot{V}$ is negative semidefinite for $K_{vs} > 0$. Again, to show global stability of the end-effector, $\dot{V}$ must be shown to be negative definite. This can be shown in a manner similar to that given for stiffness control, and therefore for brevity it will not be given (for the interested reader, see ref. 1).

Only global stability of the end-effector has been shown. To show global stability of the entire manipulator, additional damping terms must be added, as given in Eq. (2.20).

5.4 POSITION-POSITION CONTROL

For local positional stability of the position-position controller, assume the Coriolis and centrifugal effects in Eq. (1.1) can be neglected [which appears to be a good assumption; see ref. 20-25]. Further, with the assumptions that the gravity torques have been compensated for and the external forces are zero, Eq. (1.1) simplifies to

$$M_s \ddot{q} = \tau_s \ , \tag{5.28}$$

with a slave torque signal of

$$\tau_s = K_{ps}(q_s^D - q_s) + K_{vs}(\dot{q}_s^D - \dot{q}_s) \ . \tag{5.29}$$

Linearizing Eqs. (5.28) and (5.29) about a nominal position q_s^D gives

$$M_s \delta \ddot{q}_s = -K_{ps}(\delta q_s) - K_{vs}(\dot{\delta} q_s) \ , \tag{5.30}$$

where $\delta q_s = q_s - q_s^D$.

M_s is positive definite, and if K_{ps} and K_{vs} are made positive definite, then Eq. (5.30) is asymptotically stable.[9] A local stability is therefore proved.

Equation (5.30) can be put into the state space format,

$$\dot{\delta x} = A\,\delta x \quad , \tag{5.31}$$

where

$$A = \begin{bmatrix} 0 & I \\ -M_s^{-1} K_{ps} & -M_s^{-1} K_{vs} \end{bmatrix} , \tag{5.32}$$

$$\delta x = \left[\delta q_s, \dot{\delta} q_s\right]^T \quad .$$

5.5 HYBRID CONTROL

For local positional stability of the hybrid controller, the same assumption as for the position-position control will be used, and Eq. (5.28) will represent the manipulator dynamics with a slave torque signal of

$$\tau_s = K_{ps} J_s^+(x_m - x_s) + K_{vs} J_s^+(\dot{x}_m - \dot{x}_s) - k_{vnull}(I - J_s^+ J_s)\,\dot{q}_s \quad , \tag{5.33}$$

where the null motion stabilization signal has been included. Linearizing Eqs. (5.28) and (5.33) about a nominal position q_s^D where $x_m = KIN\, q_s^D$,

$$M_s \delta \ddot{q}_s = -K_{ps} J_s^+ \Delta x_s - K_{vs} J_s^+ \dot{\Delta} x_s - k_{vnull}(I - J_s^+ J_s)\,\delta \dot{q}_s \quad , \tag{5.34}$$

where $\Delta x_s = x_s - x_m$ and J_s^+ is the least-square generalized inverse.

Replacing Eq. (5.34) with $\dot{\Delta} x_s = J_s\,\dot{\delta} q_s$ and $\Delta x_s = J_s\,\delta q_s$ gives

$$M_s \delta \ddot{q}_s = -K_{ps} J_s^+ J_s\,\delta q_s - K_{vs} J_s^+ J_s\,\dot{\delta} q_s - k_{vnull}(I - J_s^+ J_s)\,\dot{\delta} q_s \quad . \tag{5.35}$$

Define the following two projection matrices:

$$P = (I - J_s^+ J_s) \text{ and } Q = J_s^+ J_s \quad .$$

These matrices have the properties that $L = \{P\, v\colon v \in R^n\}$ and $L^\perp = \{Q\, v\colon v \in R^n\}$ are orthogonal linear subspaces. Any point $v \in R^n$ can be represented uniquely as $v = p + q$, where $p \in L$ and $q \in L^\perp$.

Decompose $\dot{\delta} q_s$ into

$$\dot{\delta} q_s = \dot{\delta} q_s^\perp + \dot{\delta} q_s^{null} \quad , \tag{5.36}$$

where $\dot{\delta} q_s^\perp \in L^\perp$ and $\dot{\delta} q_s^{null} \in L$. Then Eq. (5.35) simplifies to

$$M_s \delta \ddot{q}_s = -K_{ps}\, Q\, \delta q_s - K_{vs} \dot{\delta} q_s^\perp - k_{vnull} \dot{\delta} q_s^{null} \quad . \tag{5.37}$$

The damping terms in Eq. (5.37) can be shown to be dissipative for any nonzero joint velocity if K_{ps} and K_{vs} are made positive definite. Then Eq. (5.37) is asymptotically stable.[9] Local stability is therefore proved.

6. UNMODELED DYNAMICS

6.1 BACKDRIVABILITY

6.1.1 Background

The backdrivability problem is that situation, opposite to normal robotic operation, in which mechanical power is flowing from the end-effector to the actuators. The prime mover in this case is either a human operator or an environmental force. From a design point of view, it is desirable that forces or torques required to backdrive the manipulator be as low as possible. Typical industrial robots are not backdrivable because of large frictional forces at the actuators and joints. Backdrivability forces are designed to be lower for teleoperated systems than for industrial robotic manipulators by allowing for more backlash and less stiffness. Unfortunately, the teleoperator system then has poor positional accuracy and repeatability. The degree of backdrivability is one of the fundamental differences between a teleoperator and an industrial robot.

Backdrivability is essential for both teleoperator and robotic systems. For teleoperator systems, mechanical power flow in both directions is a normal situation, and backdrivability has been recognized from the beginning as essential for successful operation. For industrial robotic systems, backdrivability is also essential to achieve force control capability. The force control problem is concerned with applying a fixed force to an object, or maintaining a fixed impedance between the forces applied to an object, and the relative end-effector displacement. Mechanical power can flow in both directions, and that capability is one of the reasons why the present generation of mechanical robot manipulators has poor performance when force control is implemented. If an industrial manipulator is going to be operated as a teleoperator, then its backdrivability needs to be enhanced.

The following section examines the generic backdrivability problem for industrial manipulators, but designers of teleoperator manipulators will also be interested because the trade-off between backdrivability and positional accuracy becomes less significant (i.e., positional accuracy should be the dominant concern of the designer; backdrivability of the manipulator will be achieved by the joint controllers). Friction will be compensated for by means of torque/force sensing, the motivation for which will be discussed later. Two situations will be examined. The first entails the redesign of each joint to include a joint torque sensor. The second requires the application of a force torque sensor at the end-effector and the use of that signal to compensate for the joint friction.

6.1.2 Joint Control

6.1.2.1 Joint torque sensors in case 1

Placement of a torque sensor at each joint will be examined first. This case was examined by Luh et al.,[21,22] but they examined only the backlash nonlinearity of the system. Other nonlinearities due to motor saturation, gear boxes, coulomb friction and stiction effects were completely ignored. Unfortunately, these are the dominant nonlinearities of any mechanical manipulator, according to Good et al.[23] These nonlinearities will be taken into account to put the result of this study on a more credible foundation.

The block diagram for a single joint controller, assuming an independent PD controller, is shown in Fig. 6.1. Five nonlinear terms take into account the major nonlinearities of a joint controller. These nonlinearities are as follows:

1. motor saturation—NLSat,
2. motor friction due to coulomb and stiction effects—NLFm,
3. backlash due to the gear box—NLB,
4. gear box nonlinearities due to direction of power flow (more will be said later about this nonlinearity)—NLGB, and
5. load friction due to coulomb and stiction effects—NLFl.

To understand why the torque sensor compensates for the friction of the joint (really, only the motor friction), first a linear analysis will be performed, to be used only for motivational purposes, and then a detailed nonlinear analysis will be presented.

For the linear analysis, remove the nonlinear terms due to coulomb friction and stiction. Replace the nonlinear gear box, backlash, and motor saturation function with a unit gain block. Set the load torque, TL, to a unit step. Further, disconnect the PD controller by setting both Kp and Kv to zero. The governing equations describing the joint dynamics seen in the block diagram are:

$$\tau_e = -K_T K_{tor} T_s \ ; \tag{6.1}$$

$$J_m \ddot{\theta}_m = \tau_e - K_{vm} \ddot{\theta}_m - \frac{T_s}{n} \ ; \tag{6.2}$$

$$T_s - T_L = J_L \ddot{\theta}_L + K_{VL} \ddot{\theta}_L \ ; \tag{6.3}$$

$$T_s = K_s \left(\frac{\theta_m}{n} - \theta_L \right) . \tag{6.4}$$

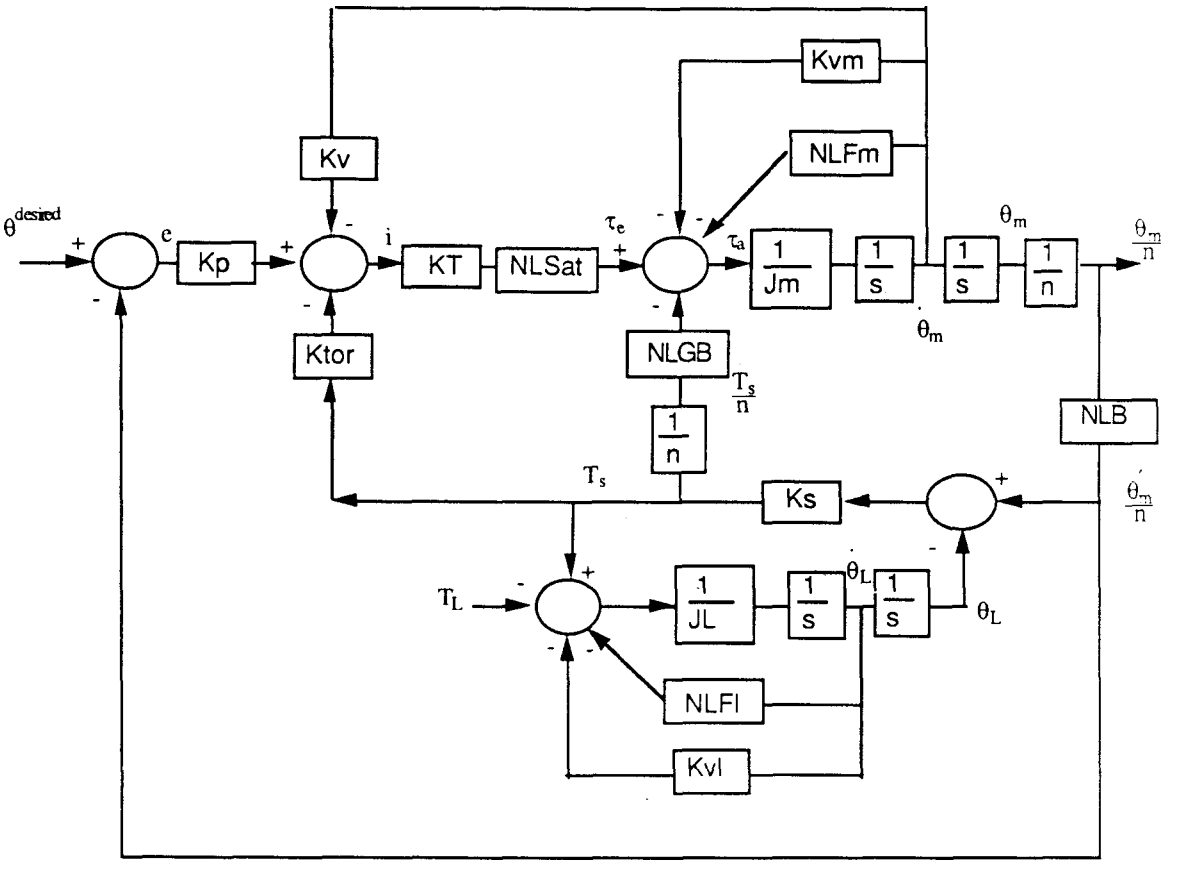

Fig. 6.1. Block diagram showing joint nonlinearities.

The transfer function relating the motor velocity to load torque TL can be derived from these equations without resorting to Mason's gain rule. First, take the Laplace transform of Eqs. (6.1) through (6.4), then substitute Eq. (6.4) into Eq. (6.3):

$$n(J_L s^2 + K_{VL} s + K_s)\theta_L = K_s \theta_m - nT_L \ . \tag{6.5}$$

Substitute Eq. (6.1) into Eq. (6.2):

$$(n\, J_m\, s^2 + nK_{vm}\, s)\ \theta_m = -\ (n\, K_T\, K_{tor} + 1)\ T_s \ ; \tag{6.6}$$

then, substitute Eq. (6.4) into Eq. (6.6):

$$\{n^2\, J_m\, s^2 + n^2\, K_{vm}\, s + (n\, K_T\, K_{tor} + 1)\, K_s\}\ \theta_m = n(n\, K_T\, K_{tor} + 1)\, K_s\, \theta_L \ . \tag{6.7}$$

Now, solve Eq. (6.7) for load angle θ_L:

$$\theta_L = \frac{\{n^2 J_m s^2 + n^2 K_{vm} s + (n K_T K_{tor} + 1) K_s\}}{n(n K_T K_{tor} + 1) K_s} \theta_m \quad . \tag{6.8}$$

Substitute Eq. (6.8) into Eq. (6.5) and collect the T_L and θ_m terms:

$$- T_L = \frac{1}{n}\left\{\frac{(J_L s^2 + K_{VL} s + K_s)[n^2 J_m s^2 + n^2 K_{vm} s + (n K_T K_{tor} + 1) K_s]}{(n K_T K_{tor} + 1) K_s} - K_s\right\}\theta_m \quad . \tag{6.9}$$

After some rearrangement of Eq. (6.9), the transfer function relating T_L and $\dot{\theta}_m$ is

$$\frac{s\,\theta_m}{-T_L} = \frac{n(n K_T K_{tor} + 1)}{[K_{VL}(n K_T K_{tor} + 1) + n^2 K_{VM} + A s + B s^2 + C s^3]} \quad , \tag{6.10}$$

where A, B, and C are constants that do not have to be dealt with for this phase of the problem (the reason will become clear when the steady state motor velocity is found).

Now, if load torque T_L is a unit step, then the steady state value of the motor velocity is simply

$$\dot{\theta}_m^{ss} = \frac{-n(n K_T K_{tor} + 1)}{[K_{VL}(n K_T K_{tor} + 1) + n^2 K_{VM}]} \quad , \tag{6.11}$$

which also explains why the A, B, and C terms were not important. Equation (6.11) can be rewritten as

$$\dot{\theta}_m^{ss} = \frac{-n}{\left[K_{VL} + \dfrac{n^2 K_{VM}}{(n K_T K_{tor} + 1)}\right]} \quad . \tag{6.12a}$$

The steady state load velocity is just the steady state motor velocity divided by the gear ratio, n:

$$\dot{\theta}_L^{ss} = \frac{-1}{\left[K_{VL} + \dfrac{n^2 K_{VM}}{(n K_T K_{tor} + 1)}\right]} \quad . \tag{6.12b}$$

If $K_{tor} = 0$, then Eq. (6.12b) says that the steady state load velocity is

$$\dot{\theta}_L^{ss} = \frac{-1}{[K_{VL} + n^2 K_{VM}]} \quad , \tag{6.13}$$

and if $K_{tor} = \infty$, then the steady state motor load velocity is

$$\dot{\theta}_L^{ss} = \frac{-1}{K_{VL}} \quad . \tag{6.14}$$

For most mechanical manipulators, motor friction seen at the joint is much greater than joint friction, or, expressed mathematically,

$$n^2K_{VM} \gg K_{VL} \quad . \tag{6.15}$$

Using Eq. (6.15), Eqs. (6.13) and (6.14) say simply that to reduce the motor friction, which is the dominant friction, set the torque sensor feedback gain to as high a value as possible to achieve a significant reduction in the effective friction during the backdrivability condition.

The characteristic equation of this system using Eq. (6.9) is

$$s^4(n^2J_m J_L) + s^3 (n^2J_L K_{vm} + n^2J_m K_{VL}) + s^2 [n^2K_{VL} K_{vm} + n^2J_m K_s + J_L K_s (nK_TK_{tor} + 1)]$$

$$+ [n^2K_{vm} K_s + K_{VL}K_s (nK_TK_{tor} + 1)] = 0 \quad . \tag{6.16}$$

The Routh stability criteria can be easily applied, and they will show that this system will always be stable if all of the feedback gains are positive. However, when nonlinear terms are included, stability is no longer guaranteed. This aspect will be examined later.

6.1.2.2 End effector torque sensors in case 2

The second case to be considered is that in which a force/torque transducer is at the end-effector. The block diagram Fig. 6.2 is similar to Fig. 6.1 except that the load torque is fed directly back.

The linear analysis for this case is similar to the previous case, so details will not be repeated. The steady state load velocity is

$$\dot{\theta}_L^{ss} = \frac{-1}{\left[\dfrac{K_{VL} + n^2K_{VM}}{\left(\dfrac{n\,K_T\,K_{tor}}{K_s} + 1\right)}\right]} \quad . \tag{6.17}$$

If $K_{tor} = 0$, then Eq. (6.17) says that the steady state load velocity is

$$\dot{\theta}_L^{ss} = \frac{-1}{[K_{VL} + n^2K_{VM}]} \quad , \tag{6.18}$$

which is identical to the previous case, and if $K_{tor} = \infty$, then the steady state motor load is

$$\dot{\theta}_L^{ss} = -\infty \quad . \tag{6.19}$$

Equation (6.19) tells us that to compensate for all the joint friction, a force/torque transducer at the end-effector should be used if the torque feedback gain K_{tor} can be set to a high enough value. Unfortunately, as we shall find out later, too high a setting will

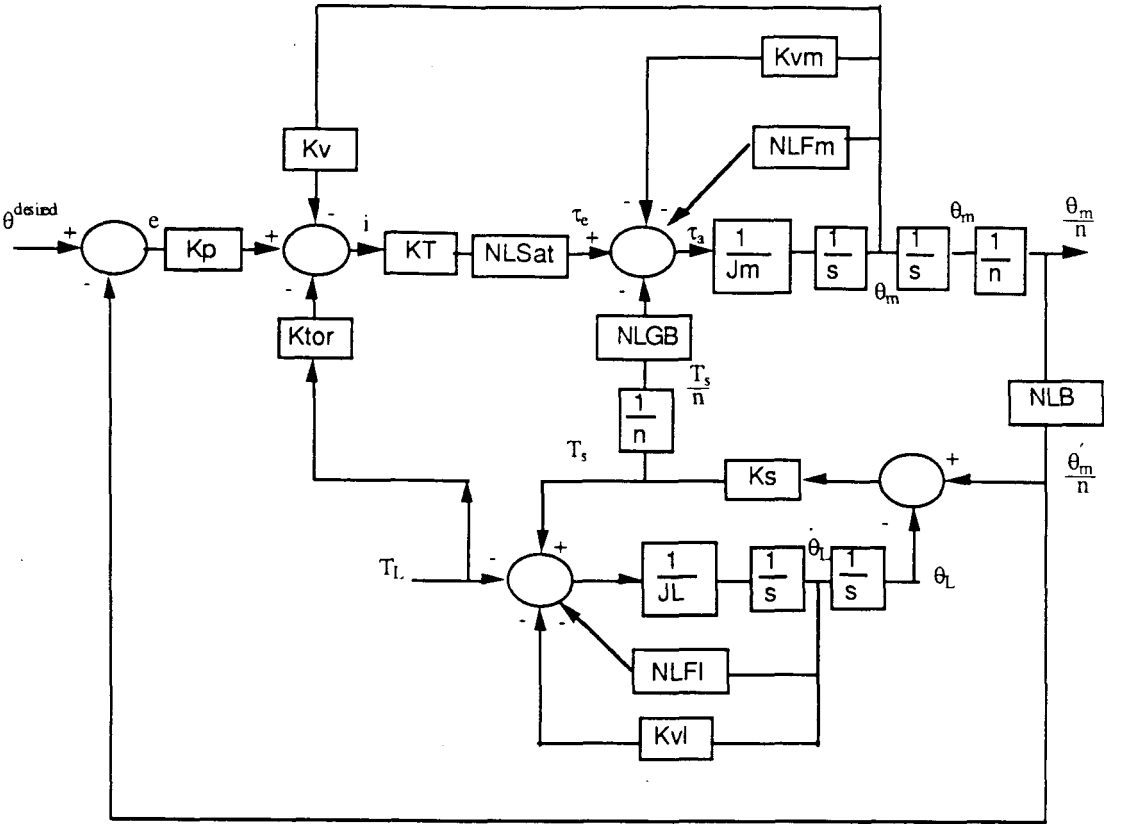

Fig. 6.2. Block diagram of joint controller with force/torque transducer.

cause a significant limit cycle[21] to be created, but further compensation can rectify this situation.

As before, if the characteristic equation for Case 2 is examined by means of the Routh stability criteria, it can be easily shown that for a linear analysis this system will, again, be stable if all feedback gains are positive. However, when the nonlinear terms are included, stability is no longer guaranteed.

6.1.2.3 Nonlinear analysis using describing functions

When the nonlinear terms are included in the analysis, three results appear possible. The first is that the system will be stable and the torque gain can be set to as high a value as possible. The second is that, as the torque gain is increased, the system will go into a limit cycle. The third is that the system will go unstable in the sense of Liapunov. Almost every book on servomechanisms claims and years of experience show that the torque gain cannot be set to any arbitrary value; thus, any possibility of the first result is eliminated. In practice, limit cycles occur when this gain is set too high.[22] The last result also is not possible, for only a finite torque can be produced by the actuator because of the saturation nonlinearity. Only uncontrolled oscillations are possible; therefore, only the second result can be achieved.

Unlike linear analysis, closed-form solutions, which include the nonlinear terms, are not possible, but accurate approximate techniques are when limit cycles are present. Techniques such as averaging or describing function (DF) methods are particularly effective. Similar to those of Luh,[21] describing techniques will be applied with all the nonlinearities included in this analysis. When only one nonlinearity exists, DFs are relatively easy to apply; when more than one exists, the analysis becomes difficult, but still is manageable if a digital computer is used. Each nonlinear term will be discussed in the following sections, then the equivalent DF will be generated. Next, limit cycle solutions will be generated for various torque gain settings that will determine the amplitude and frequency of the oscillations. Finally, a compensator will be designed based on this analysis, either to reduce the limit cycle amplitude or to remove it altogether.

The following assumptions are made in the analysis:[9,24]

1. The nonlinear elements are time-invariant.

2. The limit cycle can be approximated by a time-varying sinusoidal expression.

3. The filter hypothesis applies (i.e., higher harmonics of the limit cycle are filtered to such an extent that only a trivial quantity is fed back).

4. No subharmonics are generated.

5. The NLFl term will be set to zero because the dominant nonlinear frictions are at the motor and not the joint; however, the effect of NLFl can be easily included in the analysis.

6. The nonlinear backlash term will be modeled using the friction-controlled model. Inertia effects can be included, but for this study their effects were not considered significant.

6.1.2.3.1 Nonlinear motor friction (NLFm) DF. The NLFm friction term is due to coulomb friction and stiction of the motor. The friction will be approximated as a constant coulomb friction term with a small stiction term superimposed. This friction effect is represented in Fig. 6.3.

The DF for the NLFm term can be obtained by applying a sinusoidal motor velocity input (i.e., $\dot{\theta}_m = A_i \sin\omega t$) into this term and then taking the first harmonic component of the friction forces. Let y be the friction forces generated by a sinusoidal motor velocity input:

$$y = NLF_m\left(\dot{\theta}_m\right)$$

or

$$y = NLF_m(A_i \sin\omega t) \quad , \tag{6.20}$$

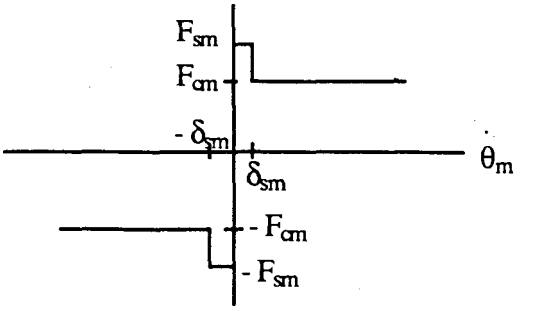

Fig. 6.3. Nonlinear friction effect.

where

A_1 = amplitude of the motor velocity,

ω = angular frequency of the limit cycle.

A_1 and ω are the unknowns that need to be found.

Now take the first harmonic component of the output, y, as

$$\frac{2}{T}\int_0^T y \sin\omega t \, dt = \begin{cases} \dfrac{4F_{sm}}{\pi} & \text{for } A_1 < \delta_{sm} \\ \dfrac{4F_{sm}}{\pi} + 1 - \sqrt{1 - \left(\dfrac{\delta_{sm}}{A_1}\right)^2} & \text{for } A_1 < \delta_{sm} \end{cases}$$

and

$$\frac{2}{T}\int_0^T y \cos\omega t \, dt = 0 \ ,$$

since NLFm is an odd function.

The DFs can now be determined to be

$$n_{pFM} = \frac{2}{A_1 T}\int_0^T y \sin\omega t \, dt = \begin{cases} \dfrac{4F_{sm}}{A_1\pi} & \text{for } A_1 < \delta_{sm} \\ \dfrac{4F_{sm}}{A_1\pi} + 1 - \sqrt{1 - \left(\dfrac{\delta_{sm}}{A_1}\right)^2} & \text{for } A_1 \geq \delta_{sm} \end{cases} \tag{6.21}$$

and

$$n_{qFM} = 0 \ . \tag{6.22}$$

Equations (6.21) and (6.22) are valid DFs for both Cases 1 and 2.

6.1.2.3.2 Backlash nonlinearity (NLB) DF. Without going into the details, as in the last DF derivation, the input into the nonlinear backlash function, NLB, is

$$\frac{\theta_m}{n} = \frac{A_1}{n\omega} \sin(\omega t - 90) \quad . \tag{6.23}$$

The nonlinear backlash DF is[3]

$$n_{pB} = 0.5\left\{1 + f\left[1 - \left(\frac{bn\omega}{A_1}\right)\right]\right\} \quad , \tag{6.24}$$

and

$$n_{qB} = \frac{-1}{\pi}\left[\frac{2bn\omega}{A_1} - \left(\frac{bn\omega}{A_1}\right)^2\right] \quad , \tag{6.25}$$

where f is saturation defined as[3]

$$f(\gamma) = \begin{cases} -1 & \text{for } \gamma < -1 \quad , \\ \frac{2}{\pi}\left(\sin^{-1}\gamma + \gamma\sqrt{1-\gamma^2}\right) & \text{for } |\gamma| \le 1 \quad , \\ +1 & \text{for } \gamma > -1 \quad , \end{cases} \tag{6.26}$$

and b is the amount of backlash.

Equations (6.24) and (6.25) are valid DFs for both Cases 1 and 2.

6.1.2.3.3 Motor saturation (NLSAT) DF. Let spring torque T_s be described as

$$T_s = n\, A_2 \sin(\omega t + \beta_2) \tag{6.27}$$

and the $(\theta_m')/n$ term as

$$\frac{\theta_m'}{n} = A_3 \sin(\omega t + \beta_3) \quad , \tag{6.28}$$

where

A_2 and A_3 are both functions of A_1 and ω,

β_2 and β_3 are both functions of A_1 and ω.

The relationship between A_2, A_3, β_2, and β_3 to A_1 and ω will be developed later, but for now assume that they are known.

Motor current i is:

$$i = -K_{tor}\, T_s - K_v\, \dot{\theta}_m - K_p \frac{\theta_m'}{n} \quad , \tag{6.29}$$

where $\theta^{desired} = 0$ for convenience. Insert Eqs. (6.27), (6.28), and $\dot{\theta}_m = A_1 \sin\omega t$ into Eq. (6.29) and combine the three phasor quantities into

$$i = A_4 \sin(\omega t + \beta_4) \quad , \tag{6.30}$$

where

$$A_4^2 = (K_{tor}\, n\, A_2 \cos\beta_2 + K_v A_1 + K_p A_3 \cos\beta_3)^2 + (K_{tor}\, n\, A_2 \sin\beta_2 + K_p A_3 \sin\beta_3)^2 \tag{6.31}$$

and

$$\beta_4 = \text{ATAN2}\,[-(K_{tor}\, n\, A_2 \sin\beta_2 + K_p A_3 \sin\beta_3) \;, \; -(K_{tor}\, n\, A_2 \cos\beta_2 + K_v A_1 + K_p A_3 \cos\beta_3)] \quad . \tag{6.32}$$

Motor electrical torque τ_e is:

$$\tau_e = \text{NLSat}\,(KT\, i) \quad , \tag{6.33}$$

and the associated DF is[24]

$$n_{pSat} = f\left(\frac{T_{max}}{A_4\, KT}\right) \quad , \tag{6.34}$$

$$n_{qSat} = 0 \quad . \tag{6.35}$$

The above derivation will generate a valid DF for Case 1. For Case 2, simply set K_{tor} to 0 in Eqs. (6.31) and (6.32).

6.1.2.3.4 Gear box nonlinearity (NLGB) DF. From Fig. 6.1, the input to the NLGB block is

$$\frac{T_s}{n} = A_2 \sin(\omega t + \beta_2) \quad . \tag{6.36}$$

The nonlinear gear box model is derived as in ref. 25. The model is dependent on the direction of power flow in the gear box. Figure 6.4 shows the nonlinear effect of the power flow. Not only is there an offset c, but the slope of the curve can change. The μ term in the figure is the coulomb friction coefficient.

Since the torsional spring torque being fed back through the gear box, T_s/n, is the in Fig. 6.4, the output of the NLGB term will be T_{in}, that is,

$$T_{in} = \text{NLGB}(T_{out}) \quad . \tag{6.37}$$

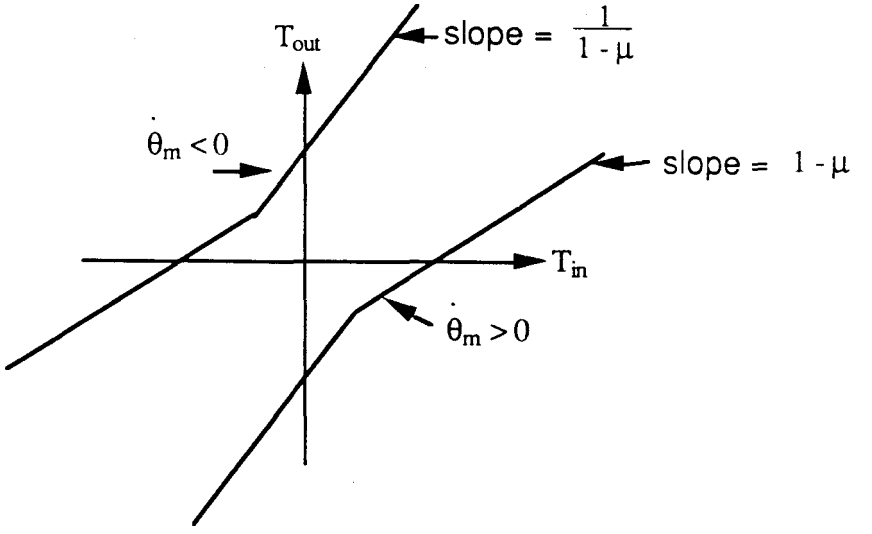

Fig. 6.4. Nonlinear input-output relationship of gear box.

Since $\dot{\theta}_m = A_1 \sin\omega t$ is positive for half the period of the sinusoid and negative for the second half, Eq. (6.37) can be determined by using the bottom curve for the first half of the period and the top curve for the last half, as shown in Fig. 6.4.

For $\dot{\theta}_m > 0$ (i.e., $0 < t < T/2$), T_{in} is:

$$T_{in} = \frac{A_2 \sin(\omega t + \beta_2)}{1-\mu} + T_{NL}, \text{ for } A_2 \sin(\omega t + \beta_2) > -c \ , \tag{6.38}$$

or

$$T_{in} = (1-\mu)[A_2 \sin(\omega t + \beta_2) + T_{NL}], \text{ for } A_2 \sin(\omega t + \beta_2) < -c \ . \tag{6.39}$$

For $\dot{\theta}_m < 0$ (i.e., $T/2 < t < T$), T_{in} is:

$$T_{in} = (1-\mu)[A_2 \sin(\omega t + \beta_2) - T_{NL}], \text{ for } A_2 \sin(\omega t + \beta_2) > c \tag{6.40}$$

or

$$T_{in} = \frac{A_2 \sin(\omega t + \beta_2)}{1-\mu} - T_{NL}, \text{ for } A_2 \sin(\omega t + \beta_2) < c \ . \tag{6.41}$$

Next, calculate the following terms:

$$a_1 = \frac{2}{T}\left[\int_0^{0.5T} T_{in} \sin\omega t \, dt + \int_{0.5T}^{T} T_{in} \sin\omega t \, dt\right] \ , \tag{6.42}$$

$$b_1 = \frac{2}{T}\left[\int_0^{0.5T} T_{in} \cos\omega t \, dt + \int_{0.5T}^{T} T_{in} \cos\omega t \, dt\right] \ . \tag{6.43}$$

Then DF for the gear box can be derived as

$$n_{pGB} = \frac{\sqrt{a_1^2 + b_1^2}}{A_2} \cos(\alpha - \beta_2) \quad , \tag{6.44}$$

and

$$n_{pGB} = \frac{\sqrt{a_1^2 + b_1^2}}{A_2} \sin(\alpha - \beta_2) \quad , \tag{6.45a}$$

where

$$\alpha = \text{ATAN2}(b_1, a_1) \quad . \tag{6.45b}$$

Equations (6.44) and (6.45) are valid DFs for Cases 1 and 2.

6.1.2.3.5 Determining: A_2, A_3, β_2, and β_3. Let us first determine A_3 and β_3 in terms of A_1 and ω. From Eq. (6.23), the input to the NLB block is

$$\frac{\theta_m}{n} = \frac{A_1}{n\omega} \sin(\omega t - 90) \quad , \tag{6.46}$$

and the output is

$$\frac{\theta'_m}{n} = A_3 \sin(\omega t + \beta_3) \quad , \tag{6.47}$$

where the higher harmonics have been ignored because of the filter hypothesis.

Using Eqs.(6.24) and (6.25), A_3 and β_3 can now be determined:

$$A_3 = \frac{A_1}{n\omega} \sqrt{n_{qB}^2 + n_{pB}^2} \quad , \tag{6.48}$$

$$\beta_3 = \alpha_2 - 90^\circ \quad , \tag{6.49}$$

where

$$\alpha_2 = \text{ATAN}_2(n_{qB}, n_{pB}) \quad . \tag{6.50}$$

Next, A_2 and β_2 will be found in terms of A_1 and ω. First, the transfer function G_1 relating T_s and $(\theta'_m)/n$ is needed. This transfer function is simply

$$G_1 = \frac{T_s}{\frac{\theta'_m}{n}} = \frac{s\, K_s (J_L\, s + K_{vl})}{J_L\, s^2 + K_{vl}\, s + K_s} \quad . \tag{6.51}$$

Replacing s with $j\omega$, $G_1(j\omega)$:

$$G_1(j\omega) = |G_1| \angle \theta_{G1} \quad , \tag{6.52}$$

where

$$|G_1| = \frac{|K_s|\sqrt{(J_L\omega^2)^2 + (K_{vl}\omega)^2}}{\sqrt{(K_s - J_L\omega^2)^2 + (K_{vl}\omega)^2}} \quad , \tag{6.53}$$

and

$$\theta_{G1} = \text{ATAN2}[K_{vl}\omega, -J_L\omega^2] - \text{ATAN2}[K_{vl}\omega, (K_s - J_L\omega^2)] \quad . \tag{6.54}$$

Since $T_s/n = A_2 \sin(\omega t + \beta_2)$, and using Eqs. (6.47), (6.48), and (6.52), A_2 is:

$$A_2 = |G_1| A_3 \quad , \tag{6.55}$$

or

$$A_2 = \frac{A_1}{n\omega}\sqrt{n_{qB}^2 + n_{pB}^2}\ \frac{|K_s|\sqrt{(J_L\omega^2)^2 + (K_{vl}\omega)^2}}{\sqrt{(K_s - J_L\omega^2)^2 + (K_{vl}\omega)^2}} \quad . \tag{6.56}$$

Likewise, β_2 is:

$$\beta_2 = \beta_3 + \theta_{G1} \quad , \tag{6.57}$$

or

$$\beta_2 = \alpha_2 - 90° + \text{ATAN2}[K_{vl}\omega, -J_L\omega^2] - \text{ATAN2}[K_{vl}\omega, (K_s - J_L\omega^2)] \quad . \tag{6.58}$$

6.1.2.3.6 Limit cycle prediction. Now, if all of the assumptions are satisfied, the DF method allows each nonlinear block in Figs. 6.1 and 6.2 to be replaced with its linear equivalent (i.e., DF) model. Both Cases 1 and 2 will be analyzed to determine the basic governing equations that predict at which amplitude and frequency the limit cycle will occur.

From Fig. 6.1, the governing equations describing the joint dynamics for Case 1 as seen from the block diagram are:

$$s\,\theta_m = G_2\,\tau_a \quad , \tag{6.59}$$

$$\tau_a = \tau_e - \text{NLFM}\ s\,\theta_m - \text{NLGB}\ T_s \quad , \tag{6.60}$$

$$\tau_e = \text{NLSat}\ K_T\, i \quad , \tag{6.61}$$

$$i = -K_v s\theta_m - K_{tor}\,T_s + K_p\, e \quad , \tag{6.62}$$

$$e = \theta^{desired} - \frac{\theta_m'}{n} \quad , \tag{6.63}$$

$$T_s = G_1 - \frac{\theta_m'}{n} \quad , \tag{6.64}$$

$$\frac{\theta_m'}{n} = NLB \frac{\theta_m}{n} \quad , \tag{6.65}$$

where

$$G_2 = 1/(J_m s + K_{vm}) \quad ,$$

$$s = j\omega \quad .$$

After some algebraic manipulation of Eqs. (6.59) to (6.65) and setting $\theta^{desired}$ to zero, one equation in terms of θ_m can be derived and is as follows:

$$\theta_m \left\{ 1 + G_2 \left[NLSat\ KT \left(K_v + K_{tor} \frac{G_1}{s} \frac{NLB}{n} + K_p \frac{NLB}{s\,n} \right) + NLFM + NLGB \frac{G_1}{s} \frac{NLB}{n^2} \right] \right\} = 0 \tag{6.66}$$

The characteristic equation is simply the terms within the braces of Eq. (6.66):

$$1 + G_2 \left[NLSat\ KT \left(K_v + K_{tor} \frac{G_1}{s} \frac{NLB}{n} + K_p \frac{NLB}{s\,n} \right) + NLFM + NLGB \frac{G_1}{s} \frac{NLB}{n^2} \right] = 0 \quad . \tag{6.67}$$

Since Eq.(6.67) is an equation of complex terms, both the real and imaginary parts must be equal to zero. This gives us two equations with two unknowns (i.e., A_1 and ω).

From Fig. 6.2, the governing equations describing the joint dynamics for Case 2 as seen from the block diagram are:

$$s\theta_m = G_2 \tau_a \quad , \tag{6.68}$$

$$\tau_a = \tau_e - NLFM\ s\theta_m - NLGB\ T_s \quad , \tag{6.69}$$

$$\tau_e = NLSat\ K_T\, i \quad , \tag{6.70}$$

$$i = -K_v s\theta_m - K_{tor}\, T_L + K_p e \quad , \tag{6.71}$$

$$e = \theta^{desired} - \frac{\theta_m'}{n} \quad , \tag{6.72}$$

$$T_s = G_1 \frac{\theta_m'}{n} \quad , \tag{6.73}$$

$$\frac{\theta_m'}{n} = NLB \frac{\theta_m}{n} \quad . \tag{6.74}$$

After some algebraic manipulation of Eqs. (6.68) to (6.74) and setting $\theta^{desired}$ and T_L to zero, one equation in terms of θ_m can be derived and is as follows:

$$\theta_m \left\{ 1 + G_2 \left[NLSat\ KT \left(K_v + K_p \frac{NLB}{s\ n} \right) + NLFM + NLGB \frac{G_1}{s} \frac{NLB}{n^2} \right] \right\} = 0 \quad . \tag{6.75}$$

The characteristic equation is simply the terms within the braces of Eq. (6.75):

$$1 + G_2 \left[NLSat\ KT \left(K_v + K_p \frac{NLB}{s\ n} \right) + NLFM + NLGB \frac{G_1}{s} \frac{NLB}{n^2} \right] = 0 \quad . \tag{6.76}$$

The major difference between Eqs. (6.76) and (6.67) is that K_{tor} appears in Case 1 and does not appear in Case 2. This means that the setting of K_{tor} does not come into play for the determination of the limit cycle in Case 2 under conditions in which the assumptions are valid. More will be said about this later.

6.1.2.3.7 **Numerical solution.** Graphical techniques are frequently used to solve DF problems with one nonlinear element. Graphical techniques can give great insight into such problems and even suggest ways of compensating the system for improved performance. For multiple nonlinearities, however, such techniques are difficult to apply. Equation (6.67) for Case 1 can be reformulated by putting the NLB term on the right-hand side:

$$\frac{G_2 \left[NLSat\ KT \left(K_{tor} \frac{G_1}{s} \frac{1}{n} + K_p \frac{1}{s\ n} \right) + NLGB \frac{G_1}{s} \frac{1}{n^2} \right]}{1 + G_2(NLFm + NLSat\ KT\ K_v)} = \frac{-1}{NLB} \quad ,$$

or

$$G_3 = \frac{-1}{NLB} \quad , \tag{6.77}$$

where G_3 is the first term in Eq. (6.77). The NLB term has been placed on the right hand side of Eq. (6.77) because it is considered to be a dominate nonlinear term when a limit cycle occurs. Further, if a change of variables is performed, A_1 and ω can be transformed into alpha and ω:

$$alpha \equiv \frac{bn\omega}{A_1} \tag{6.78}$$

and

$$\omega = \omega \quad . \tag{6.79}$$

Since A_1 and ω can take on only nonnegative values, the transformation is one to one, that is:

$$A_1 = \frac{b\ n\ \omega}{\text{alpha}} \quad , \tag{6.80}$$

$$\omega = \omega \quad . \tag{6.81}$$

The NLB term is now a function of only alpha, and the amount of gear backlash is relative, as can be seen from Eq. (6.78). For a solution to have physical meaning, alpha is restricted to lie between[3]

$$0 < \text{alpha} \leq 2 \quad . \tag{6.82}$$

Define h_1 (alpha, ω) to be the left side of Eq. (6.77) and h_2 (alpha) to be the right side. The problem then becomes to find all the alpha and ω such that the following two conditions are satisfied:

$$\text{Re}\ \{h_1 - h2\} = 0 \quad , \tag{6.83}$$

$$\text{Im}\ \{h_1 - h2\} = 0 \quad . \tag{6.84}$$

Since these two equations are nonlinear, solutions will have to be performed on the computer. The problem can be easily reformulated as: Find all alpha and ω such that

$$[\text{Re}(h_1 - h_2)]^2 + [\text{Im}(h_1 - h_2]^2 \leq \text{tol}$$

and

$$0 < \text{alpha} \leq 2 \quad ,$$

where

tol = some user specified tolerance.

Optimization routines to solve this type of problem are fairly common. We found that a conjugate gradient search routine works well. For practical considerations, the angular frequency ω should be restricted to lie within

$$\omega_{min} < \omega \leq \omega_{max} \quad , \tag{6.85}$$

and ω_{min} and ω_{max} are bounds specified by the user.

It should be noted that only some of the solutions to Eq. (6.77) are stable limit cycles. Whether or not a solution is stable is a somewhat difficult problem numerically, because the eigenvalue sensitivities associated with Eq. (6.77) will have to be determined. Methods to compute these sensitivities can be found in refs.[26,27] Because of the low dimensionality of this problem, all solutions to Eq. (6.77) can be tried out on a

program that will simulate the dynamic performance of this system. Stable solutions will be clearly seen; unstable solutions will be quickly damped out.

Similarly, Case 2 can be formulated as an optimization problem in an fashion identical to Case 1. Therefore, the details of the derivation will not be given. Clearly, limit cycles can be predicted, which is one of the main points of this section.

6.1.2.3.8 Lead/lag friction compensation. Friction can be compensated for by means of force/torque sensors, as discussed previously. Unfortunately, the gains for these signals cannot be set at any arbitrary level because of potential limit cycle problems. One method for eliminating or reducing their effects is to use a lead/lag compensator at the force/torque signal. For clarity, Case 1 will be discussed. Previous researchers have examined this case[21-23] and data are readily available. Case 2 should be similar. Figure 6.5 shows the plot of the magnitude vs phase of the G_3 and the $-1/NLB$ transfer function for different alpha values. Limit cycles might occur at their intersections. To reduce the effects of the limit cycle, the curves should be moved to the right, either to hit the curve at higher alpha values (i.e., the amplitude of the limit cycle is inversely proportional to the alpha magnitude [see Eq. (6.78)] or to avoid entirely any intersection at all. A lead/lag compensator can achieve this movement. Luh et al.[21] have reported that a 30-to-1 reduction in friction of the Stanford Arm is possible. While a 30-to-1 reduction in friction is not possible for every manipulator, reduction to some extent does appear to be possible, and this capability be exploited to improve the backdrivability of the manipulator.

6.2 UNMODELED DYNAMICS DISCUSSION AND COMPENSATION

All the control algorithms discussed in Sect. 6.1 assume rigid-body dynamics with linear friction and ideal actuators. Unfortunately, this situation is not valid, as mentioned before. Nonlinearities due to backlash, actuator limits, gear boxes, coulomb friction, and stiction are the dominant effects in the manipulator dynamics and compose the unmodeled dynamics. Unmodeled dynamics significantly limits the performance of advanced control algorithms, which is why simple PD and PID controllers have achieved such popularity in industry and why their performance is hard to beat. Unfortunately, PD and PID controllers do not exploit to any significant degree the knowledge of the system being controlled, and this lack is the primary reason why there is so much research to find better control schemes. If the unmodeled dynamics can be quantized, their effects can be diminished to some extent, as was seen in the section on backdrivability. However, careful measurements are needed because of the high dimensionality and complexity of the problem.

Figure 6.6 shows a nominal model $G(j\omega)$ and the error due to unmodeled dynamics $E(\hat{x},j\omega)$ at particular angular frequency ω. Once the overall transfer function of the system, $H(\hat{x},j\omega)$, has been determined, $E(\hat{x},j\omega)$ can be easily calculated by

$$E = -[I + G^{-1}(I - H^{-1})^{-1}] \quad . \tag{6.86}$$

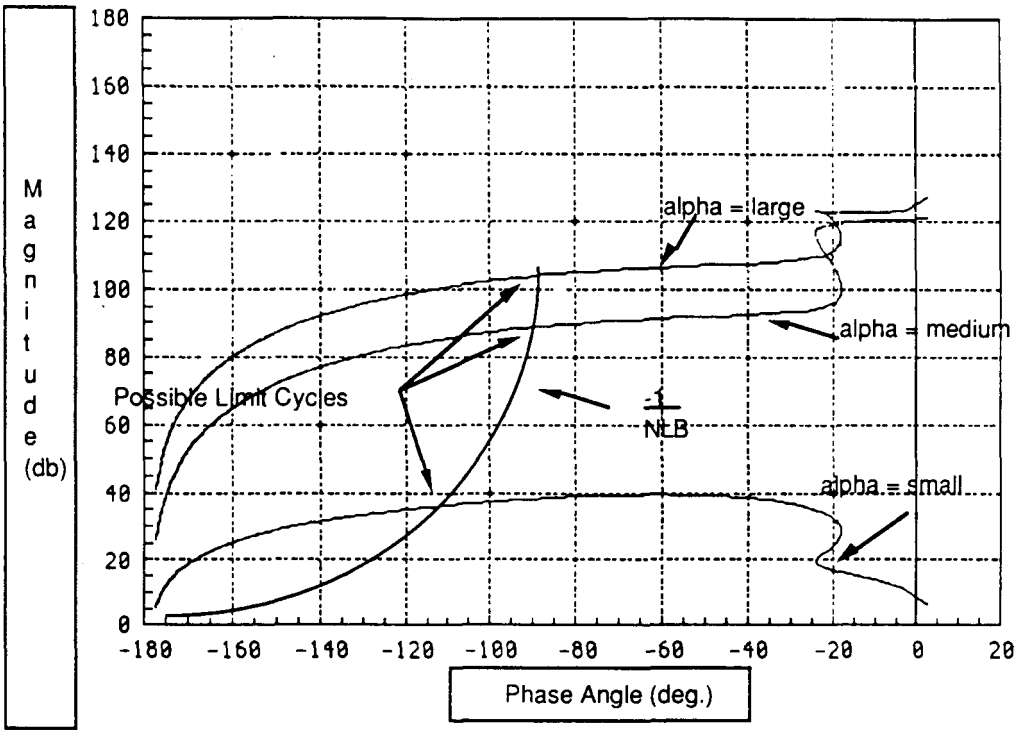

Fig. 6.5. Possible limit cycles.

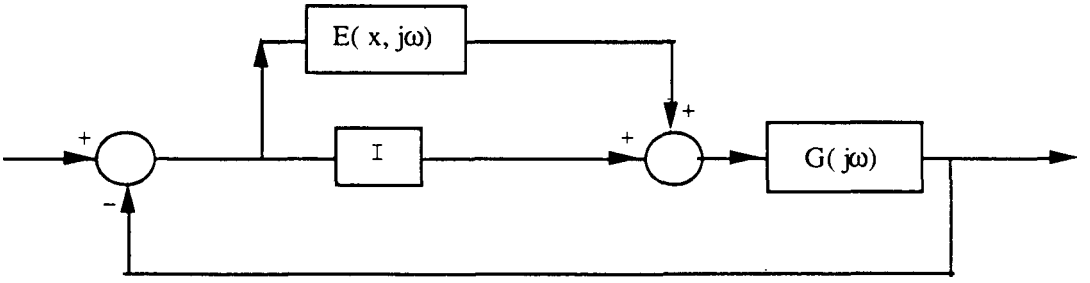

Fig. 6.6. Unmodeled dynamics model.

Once H has been measured and E calculated, the relative stability of the system can be determined, either by means of a describing function (or averaging techniques) or by stable robustness measures[16] such as

$$\|E\| < \|I + G^{-1}\| \ , \tag{6.87}$$

where $\|-\|$ is a matrix norm operator.[9] After E has been determined, a suitable compensator can be applied to limit the effects of the most relevant nonlinearities. Further, this whole process will determine regions where stable gains for the desired control can be selected.

7. SUMMARY AND CONCLUSIONS

Section 1 of this report gives an introduction to the problem of dissimilar and redundant bilateral, force-reflecting teleoperators. Section 2 gives the fundamental theory of redundant teleoperators with dissimilar kinematics. Section 3 discusses the basic philosophy of how a teleoperated system should be designed if only the slave has a force/torque sensor. Section 4 categorizes the different types of control algorithms into four basic types: position-position, hybrid, stiffness, and impedance control. Criteria to judge the relative attributes of each type are listed in Table 2. The impedance type of controller has been determined to be best in the sense that it decouples the Cartesian motions and allows for uniform and adjustable stiffness in Cartesian space. Section 5 gives a deeper discussion of the stability and transient issues of each of the controller types. Section 6 discusses unmodeled dynamics and its effects on the performance of the manipulator. It is argued that joint compensators would be designed to limit the effects of the dominant, unmodeled nonlinearities at the joint level. These joint compensators would make the manipulator appear, to some extent, to behave like a rigid body controlled by an ideal actuator. Impedance control algorithms as discussed in Sect. 3 would then be "layered" over these joint compensators. The overall effect should be a significant improvement in performance and controllability (i.e., uniform and adjustable stiffness) throughout the workspace.

REFERENCES

1. Khatib, O., "A Unified Approach for Motion and Force Control of Robot Manipulators: The Operational Space Formulation," IEEE Journal of Robotics and Automation, Vol. RA-3, No. 1, Feb. 1987, pp. 43-53.

2. Khatib, O., "Real-Time Obstacle Avoidance for Manipulators and Mobile Robots," 1985 IEEE International Conference on Robotics and Automation, pp. 500-505.

3. Whitney, D., "The Mathematics of Coordinate Control of Prosthetic Arms and Manipulators," Journal of Dynamic Systems, Measurement, and Control, 1972, pp. 303-309.

4. Dubey, R. V., Euler, J. A. and Babcock, S. M., "An Efficient Gradient Projection Optimization Scheme for a Seven-Degree-of-Freedom Redundant Robot with Spherical Wrist," 1988 IEEE International Conference on Robotics and Automation, pp. 28-36.

5. Dubey, R. and Luh, J. Y. S., "Redundant Robot Control Using Task Based Performance Measures," Journal of Robotic Systems, 5(5), 1988, pp. 409-432.

6. Chiu, S. L , "Control of Redundant Manipulators for Task Compatibility," 1987 IEEE International Conference on Robotics and Automation, pp. 1718-1724.

7. Arzbaechar, R. C., Servomechanisms with Force Control, Ph.D. Thesis at the University of Chicago, May 1960.

8. Miyazaki, F., Matsubayashi, S., Yoshimi, T. and Arimoto, S., "A New Control Methodology Toward Advanced Teleoperation of Master-Slave Robot Systems," 1986 IEEE International Conference on Robotics and Automation, pp. 997-1002.

9. Vidyasagar, M., Nonlinear Systems Analysis, Prentice-Hall, Inc. Englewood Cliffs, New Jersey, 1978.

10. Asada, H. and Slotine, J.-J.. E., Robot Analysis and Control, John Wiley and Sons, New York, N. Y., 1986.

11. An, C. H., Atkeson, C. G. and Hollerbach, J. M. , Model-Based Control of a Robotic Manipulator, MIT Press, Cambridge, Massachusetts, 1988.

12. Raibert, M. H. and Craig, J. J., "Hybrid Position/Force Control of Manipulators," Journal of Dynamic Systems, Measurement, and Control, June 1981, pp. 126-133.

13. Salisbury, J. K., "Active Stiffness Control of a Manipulator in Cartesian Coordinates," IEEE Conf. Decision and Control, Albuquerque, New Mexico, Nov. 1980, pp. 95-100.

14. Asada, H. and Youcef-Toumi, K., Direct-Drive Robots, MIT Press, Cambridge, Massachusetts, 1987.

15. Hogan, N., "Impedance Control: An Approach to Manipulation: Part 1 - Theory," Journal of Dynamic Systems, Measurement, and Control, March 1985, Vol. 107, pp. 1-7.

16. Hogan, N., "Impedance Control: An Approach to Manipulation: Part 2 - Implementation," Journal of Dynamic Systems, Measurement, and Control, March 1985, Vol. 107, pp. 8-16.

17. Hogan, N., "Impedance Control: An Approach to Manipulation: Part 3 - Applications," Journal of Dynamic Systems, Measurement, and Control, March 1985, Vol. 107, pp. 17-24.

18. Luh, J. Y. S., Walker, M. W., and Paul, R. P. C., "Resolved-Acceleration Control of Mechanical Manipulators," IEEE Transaction on Automatic Control, Vol. AC-25, No. 3, 1980.

19. Bazaraa, M. S. and Shetty, C. M., Nonlinear Programming: Theory and Algorithms, John Wiley and Sons, New York, N. Y., 1979.

20. Leahy, M. B., Valavanis, K. P. and Sardis, G. N., "Evaluation of Dynamic Models for PUMA Robot Control," IEEE Transactions on Robotics and Automation, Vol. 5, No. 2, April, 1989.

21. Luh, J. Y. S., Fisher, W. D. and Paul, R. P. C., "Joint Torque Control by a Direct Feedback for Industrial Robots," IEEE Transactions on Automatic Control, Feb. 1983, Vol. AC-28, No. 2, pp. 153-161.

22. Eppinger, S. D. and Seering, W. P., "On Dynamic Models of Robot Force Control," 1986 IEEE International Conference on Robotics and Automation, pp. 29-34.

23. Good, M. C., Sweet, L. M. and Strobel, K. L., "Dynamic Models for Control System Design of Integrated Robot and Drive Systems," Journal of Dynamic Systems, Measurement, and Control, March 1985, Vol. 107, pp. 53-59.

24. Gelb, A and Velde, W. E. V, Multiple-Input Describing Functions and Nonlinear System Design, McGraw-Hill, Inc., New York, N. Y., 1968.

25. Gogoussis, A. and Donath, M., "Coulomb Friction Joint and Drive Effects in Robot Mechanisms," 1987 IEEE International Conference on Robotics and Automation, pp. 828-836.

26. Abel, S. G. and Cooperrider, N. K., "An Equivalent Linearization Algorithm for Nonlinear System Limit Cycle Analysis," Journal of Dynamic Systems, Measurement, and Control, June 1985, Vol. 107, pp. 117-122.

27. Pillai, V. K. and Nelson, H. D., "A New Algorithm for Limit Cycle Analysis of Nonlinear Control Systems," Transaction of the ASME, Sept. 1988, Vol. 110, pp. 272-277.

BIBLIOGRAPHY

1. Asare, H. R. and Wilson, D. G., "Evaluation of Three Model Reference Adaptive Control Algorithms for Robotic Manipulators," Proceeding of 1987 IEEE International Conference on Robotics and Automation.

2. Dubowsky, S. and DesForges, D. T., "The Application of Model-Reference Adaptive Control to Robotic Manipulators," Journal of Dynamic Systems, Measurements, and Control, Vol. 101, Sept. 1979, pp. 193-200.

3. Hsia, T. C., "Adaptive Control of Robot Manipulators-A Review," Proceeding of 1986 IEEE International Conference on Robotics and Automation.

4. Landau, Y. D. , Adaptive Control-The Model Reference Approach, Marcel Dekker, Inc. , New York, 1979.

5. Nicosia, S. and Tomei, P., "Model Reference Adaptive Control Algorithm for Industrial Robots," Automatica Vol. 20, No. 5, pp. 635-644, 1984.

INTERNAL DISTRIBUTION

1-10. S. M. Babcock
11. H. R. Brashear
12. B. G. Eads
13. D. N. Fry
14. W. R. Hamel
15. J. N. Herndon
16-25. J. F. Jansen
26. R. L. Kress
27. D. W. McDonald
28. D. R. Miller
29. C. A. Mossman
30. L. C. Oakes
31. R. E. Uhrig
32. A. Zucker
33. J. B. Ball, Advisor
34. P. F. McCrea, Advisor
35. T. B. Sheridan, Advisor
36-37. Central Research Library
38. Y-12 Technical Reference Section
39-40. Laboratory Records Department
41. Laboratory Records ORNL-RC
42. ORNL Patent Section
43. I&C Division Publications Office

EXTERNAL DISTRIBUTION

44. Assistant Manager for Energy Research and Development, U.S. Department of Energy, Oak Ridge Operations Office, Oak Ridge, TN 37831.
45. Capt. Ronald G. Julian, Biological Acoustics Branch, Biodynamics and Bioengineering Division, Armstrong Aerospace Medical Research Laboratory, WPAFB, OH 45433-6573.
46. 1st Lieut. Steven J. Remis, Biological Acoustics Branch, Biodynamics and Bioengineering Division, Armstrong Aerospace Medical Research Laboratory, WPAFB, OH 45433-6573.
47-56. Office of Scientific and Technical Information, P.O. Box 62, Oak Ridge, TN 37831.